

Testing a New Star Formation History Model from Principal Component Analysis to Facilitate Spectral Synthesis Modeling

YANZHE ZHANG ¹, H.J. MO ¹, KATHERINE E. WHITAKER ¹ AND SHUANG ZHOU ²¹*Department of Astronomy, University of Massachusetts, Amherst, MA, 01003-9305, USA*²*INAF – Osservatorio Astronomico di Brera, via Brera, 28, 20159 Milano, Italy*

ABSTRACT

The spectrum of a galaxy is a complicated convolution of many properties of the galaxy, such as the star formation history (SFH), initial mass function, and metallicity. Inferring galaxy properties from the observed spectrum via spectral synthesis modeling is thus challenging. In particular, a simple yet flexible model for the SFH is required to obtain unbiased inferences. In this paper, we use SFHs from the IllustrisTNG and EAGLE simulations to test SFH models in their capabilities of describing the simulated SFHs and the spectra generated from them. In addition to some commonly used SFH models (Γ , τ , and non-parametric), we also examine a model developed from the principal component analysis (PCA) trained by a set of SFHs from IllustrisTNG. We find that when using the first 5 principal components (eigen-histories), the PCA-based model can achieve a good balance between simplicity and accuracy. Among all the SFH models, the PCA-based model is the best in matching the simulated SFHs. To accurately reproduce the spectra generated from the simulated SFHs, it is necessary to have a degree of freedom to describe the most recent SFH (e.g., a step function covering the age of 0 - 0.3 Gyr). Overall, the PCA+step model performs the best in covering the diversity of SFHs and in reproducing the input spectra, thus providing a reliable SFH model for spectral synthesis modeling.

Keywords: Astronomical models(86) – Star formation(1569) – Galaxy stellar content(621) – Galaxy evolution(594)

1. INTRODUCTION

Observationally, many physical properties of a galaxy are encoded in its spectra and usually inferred through spectral synthesis modeling (SSM). However, such modeling is extremely challenging, because the main components, such as the star formation history (SFH), initial mass function (IMF), dust, and metallicity, are highly degenerate in the synthesized spectra (see review by Conroy 2013). In particular, the SFH, one of the most crucial quantities of a galaxy related to its assembly and evolution, is strongly degenerate in the spectral space, as each stellar population at a given age contributes to the spectrum over a large range of wavelength (e.g., Thomas et al. 2005; Lee et al. 2018).

With the advent of large and deep extragalactic surveys, the cosmic star formation history, the average

star formation rate per co-moving volume as a function of cosmic time (redshift, z), is quite well established (Madau & Dickinson 2014). This history consists of a rising phase from high- z to $z \sim 2$ with a gradually declining phase to the present time. However, the SFHs of individual galaxies are diverse. For example, the quenching of star formation may be driven by different mechanisms that depend on the stellar mass of galaxies (Peng et al. 2010), thereby giving rise to systematically different SFHs (e.g. Pacifici et al. 2016; Heavens et al. 2004). More recent studies of dwarf galaxies find that their SFHs are systematically different from those of galaxies of Milky-Way mass (e.g., Weisz et al. 2011; Kauffmann 2014; Lu et al. 2014, 2015; Zhou et al. 2020). The diversity of SFH among the observed galaxy populations indicates that it is necessary to model the SFHs properly to make unbiased inferences from the observed spectra. Three qualities are needed for a successful model. First, the model should be simple, so that it can be constrained by observations. Secondly, the model should be flexible, so that it can cover the diversity in

the SFHs. Thirdly, the model should be reliable, so that it does not lead to biased predictions from the spectra. The third requirement is essential because the transformation from a SFH to a synthesized spectrum is highly nonlinear.

Various SFH models have been proposed for spectral synthesis modeling (e.g., [Carnall et al. 2019](#); [Leja et al. 2019](#); [Suess et al. 2022](#)). Some commonly used parametric models include the Γ model ([Lu et al. 2014](#)), the exponentially-declining (τ and delayed- τ) model ([Wu et al. 2018](#); [Lee et al. 2018](#); [Carnall et al. 2019](#); [Jain et al. 2024](#)), the double-power law model ([Behroozi et al. 2013](#); [Gladders et al. 2013](#); [Pacifci et al. 2016](#); [Carnall et al. 2018](#)), and the log-normal model ([Gladders et al. 2013](#)). Non-parametric models based on binning the SFH into histograms have also been used, either with fixed time bins ([Weisz et al. 2011](#); [Leja et al. 2019](#)) or with variable time bins ([Suess et al. 2022](#)). Yet the applicability and performance of these models have not been tested systematically according to the criteria described above, and it is still unclear which model is preferred in real applications (e.g., [Zhou et al. 2020](#); [Narayanan et al. 2023](#)).

To better investigate the diversity of the galaxy populations in their SFHs, we take advantage of hydrodynamic cosmological simulations that can predict the SFHs of individual galaxies. This will allow us to test directly the performance of different SFH models, as well as the spectra predicted by these SFH models in comparison to those obtained directly from the simulated SFHs. In this study, we use IllustrisTNG data, a high-resolution cosmological hydrodynamic simulation of galaxy formation ([Springel et al. 2017](#); [Nelson et al. 2017](#); [Pillepich et al. 2017a](#); [Naiman et al. 2018](#); [Marinacci et al. 2018](#)). We select all central galaxies with stellar masses larger than $1 \times 10^9 h^{-1} M_\odot$ at $z = 0$ from IllustrisTNG 100-1 simulation as our main sample. In addition to testing existing models, we also test a new set of models developed from principal component analysis (PCA); we refer to these models herein as the PCA-based models. We apply the PCA to the simulated SFHs to obtain a set of principal components (the eigenhistories) and use several lower-order eigenhistories as the base function to model the SFHs of galaxies. We demonstrate the flexibility and reliability of the PCA-based models by comparing them to existing models.

The paper is organized as follows. In §2, we introduce the training data set (IllustrisTNG) and the software (BIGS: Bayesian Inference of Galaxy Spectra) that generates the mock galaxy spectra. In §3, we introduce a few traditional SFH models we intend to test and describe our PCA-based models. In §4, we first test SFH models in their capacities to describe the input SFHs

of individual galaxies in the simulated sample. We then generate synthesized spectra using the best-fit SFHs and compare them to spectra generated by the input SFHs. We also study how the predicted spectra are affected by the presence of very recent star formation, and test how the acceptability of different models changes with the signal-to-noise ratio (SNR) of the spectra. In §5, we test the validity of the PCA-based models by applying them to galaxy samples of different properties and to galaxies from an independent hydro simulation. We further discuss and summarize our main conclusions in §6.

The cosmology model used in this paper is adopted from [Planck Collaboration et al. \(2016\)](#), which has $\Omega_{\Lambda,0} = 0.69$, $\Omega_{m,0} = 0.31$, $\Omega_{b,0} = 0.049$, and $H_0 = 100 h \text{ km s}^{-1} \text{ Mpc}^{-1}$ with $h = 0.68$. This cosmology is also used in the TNG simulation.

2. DATA AND SOFTWARE

2.1. Training Data

We use data from the publicly available IllustrisTNG project, which is a set of cosmological hydrodynamic simulations ([Springel et al. 2017](#); [Nelson et al. 2017](#); [Pillepich et al. 2017a](#); [Naiman et al. 2018](#); [Marinacci et al. 2018](#)). IllustrisTNG is built upon the moving mesh code AREPO ([Springel 2010](#)) and the success of the former Illustris galaxy formation model ([Vogelsberger et al. 2014a,b](#); [Genel et al. 2014](#); [Sijacki et al. 2015](#)). Several improvements are implemented in IllustrisTNG, including a new model of feedback effects from supermassive black holes ([Weinberger et al. 2016](#)) and some improvements in the numerical framework ([Pillepich et al. 2017b](#)).

The IllustrisTNG project includes simulations in three cubic boxes, with co-moving side lengths L_{box} roughly equal to 50 (TNG50), 100 (TNG100), and 300 (TNG300) Mpc, respectively. The largest simulation, TNG300, covers a relatively large physical volume, and thus, enables studies of galaxy clustering, rare and massive objects, and statistical analyses of galaxies. On the other hand, the smallest one, TNG50, offers a more detailed mass resolution on galaxies, which allows investigations of the structural properties of galaxies and small-scale gas processes in and around galaxies. TNG100 provides a balance between volume and mass resolution. We use the highest resolution run of the TNG100 simulation, TNG100-1 (hereafter TNG100), which simulates galaxy evolution from $z = 127$ to $z = 0$ in a box with $L_{\text{box}} \sim 110.7 \text{ Mpc}$ (75 cMpc/h). The minimum baryonic particle mass is $m_{\text{gas}} \sim 1.4 \times 10^6 M_\odot$.

We select 16,141 galaxies at $z = 0$ with a stellar mass threshold $M_* = 1.0 \times 10^9 h^{-1} M_\odot$, thereby ensuring that

these galaxies are well resolved in TNG100 at higher redshifts. The sample includes both central and satellite galaxies. We find that some of the satellite galaxies in the simulation have zero SFR at low z , partly because of the quenching of star formation by halo-specific environmental effects, and partly because of numerical difficulties to follow the evolution of satellite galaxies accurately. We, therefore, exclude satellite galaxies from the training data set, which gives a sample of 9,168 central galaxies at $z = 0$. This choice not only reduces potential impacts by numerical uncertainties in satellite galaxies but also provides an opportunity to test whether or not our approach depends significantly on the training data adopted. As shown in §5.2, the PCA-based models trained by central galaxies are also valid for satellite galaxies.

For each central galaxy at $z = 0$, a total of 100 snapshots of redshift from $z = 127$ to $z = 0$ are available. We use the SFHs only where $z \lesssim 6$, which comprises 87 snapshots. We convert redshift into cosmological time using the cosmological model adopted by the simulation. In developing the new PCA-based models in §3.2.2, we re-sample the star formation history by interpolating the TNG100 data onto a 100-point time grid in logarithmic scale (base 10) that spans the cosmic time up to $z \lesssim 6$. In Fig. 1, we show one example to demonstrate our re-sampling of the SFH. The upper panel shows the original TNG100 sampling with respect to redshift, and the lower panel includes the converted cosmological look-back time (the black line) and our new interpolated sampling (the red dots) as a function of look-back time. Whereas the original sampling emphasizes older stellar populations at higher redshifts, our new sampling gives more weight to star formation at the most recent look-back times. More details can be found in §3.

2.2. Stellar Spectra

We generate the spectral energy distribution (SED) of each galaxy from its SFH using a stellar population synthesis code, the Bayesian Inference of Galaxy Spectra (BIGS), developed by Zhou et al. (2019). BIGS utilizes a full Bayesian analysis to fit the composite spectrum of a galaxy along with several physical properties, such as the initial mass function (IMF), star formation history (SFH), metallicity (Z), and dust attenuation. This code has been applied to MaNGA data to constrain the IMF in early-type galaxies (Zhou et al. 2019), simultaneously model mass accumulation and chemical evolution for spiral galaxies (Zhou et al. 2022), the SFH of low-mass galaxies (Zhou et al. 2020), and massive red spiral galaxies (Zhou et al. 2021) in the local universe. One of our eventual goals is to implement the new PCA-based

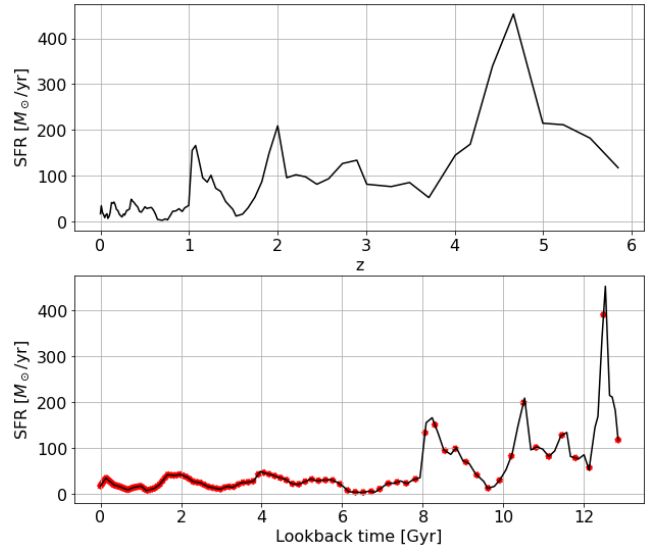


Figure 1. An example of the TNG100 SFH, sampled in the original redshift (upper panel) and in look-back time (lower panel). The solid black line is the original sampling in cosmic look-back time, and the red dots are the re-sampling in a logarithmic (10-based) time grid.

models obtained in this study into BIGS. For the purpose of this paper, however, we only use BIGS to generate mock spectra from given SFHs. We refer the reader to the above references for a more detailed description of the code and the Bayesian inferences.

BIGS provides the choices of different IMFs and templates of stellar spectra. To better isolate the effects produced by using different SFH models, we fix all parts other than the SFH, including adopting a Chabrier stellar IMF (Chabrier 2003) and the Padova 1994 isochrones (Bertelli et al. 1994), and test several SFH models as detailed in §3. Combining the simulated SFHs with the BC03 SSP templates (Bruzual & Charlot 2003), constructed with the STELIB stellar library that has a wavelength range covering 3200 - 9500 Å with a spectral resolution of ~ 3 Å (Le Borgne et al. 2003), and the Calzetti dust attenuation curve (Calzetti et al. 2000), we generate composite mock spectra for simulated galaxies in our sample. We do not include broadening produced by stellar kinematics, but we test the effects of spectral resolutions and the signal-to-noise ratio. Unless stated otherwise, we adopt a Solar metallicity and an E(B-V) value of 0.1.

3. STAR FORMATION HISTORY MODELS

In general, the SFH of a galaxy can be complicated, in the sense that it is hard to come up with a universal model for different galaxies. From the observational point of view, inferring the SFH of a galaxy from its spectrum is challenging because of the degeneracy of the

SFH with the IMF, metallicity, dust attenuation, and other factors. Consequently, inferences of SFHs from the observed spectra have to be made by adopting simple models for the functional form of the SFH. In this section, we first introduce three traditional SFH models: the Γ model, the τ model, and the non-parametric stepwise model. We then present the development of our new SFH model based on the principal component analysis (PCA).

3.1. Traditional Models

Traditionally, SFHs of galaxies are modeled by two approaches: (1) the parametric approach that assumes a functional form characterized by a small number of parameters, and (2) the non-parametric approach that models the SFH using histograms with various time bins. In this paper, we will test two parametric models, the Γ model and τ model, and a stepwise model with a given number of time bins.

The Γ model: This model is defined by a Γ function, representing the star formation rate (SFR) as a function of cosmic time t :

$$\Psi(t) = \frac{1}{\tau\gamma(\alpha, t_0/\tau)} \left(\frac{t_{\text{lb}}}{\tau}\right)^{\alpha-1} e^{-t_{\text{lb}}/\tau}, \quad (1)$$

where

$$t_{\text{lb}} \equiv t_0 - t \quad (2)$$

is the look-back time with t_0 being the present time, and

$$\gamma(\alpha, t_0/\tau) \equiv \int_0^{t_0/\tau} x^{\alpha-1} e^{-x} dx. \quad (3)$$

The model is thus specified by two free parameters, α and τ , and normalized so that $\int_0^{t_0} \Psi(t) dt = 1$. The motivation for including the Γ model comes from the empirical model of Lu et al. (2014), who found that such a model can describe the SFH of many galaxies in their empirical model of galaxy formation. Moreover, it was also implemented in BIGS to study different types of galaxies in the local universe (Zhou et al. 2020, 2021). Given that there are only two free parameters, it is one of the simplest SFH models. Yet, for the same reason, this model may introduce bias in the inferences of physical parameters because it is not very flexible (Carnall et al. 2019). We include this model in our study to test its applicability and for comparison with other models.

The τ model: This is an exponentially declining SFH, parameterized by the e-folding time τ , and has the form

$$\Psi(t) = \begin{cases} \frac{1}{\tau\gamma(1, [t_0 - t_s]/\tau)} \exp\left(-\frac{t - t_s}{\tau}\right), & t > t_s; \\ 0, & \text{otherwise,} \end{cases} \quad (4)$$

where t_s is a specific time when star formation starts from zero to the maximum value. Similar to the Γ model, this model also has two free parameters, t_s and τ . The τ model is one of the most commonly applied SFH models because of its simplicity. Although recent improvements of statistical and computational techniques allow for more complex SFH models in SED fitting, the τ model is still widely used for comparison (e.g., Wu et al. 2018; Lee et al. 2018; Carnall et al. 2019; Jain et al. 2024). However, this model seems to be disfavored by applications to high-redshift galaxies (Reddy et al. 2012) and in fitting simulated galaxies (Carnall et al. 2018; Joshi et al. 2021), as it can lead to significantly-biased inferences (Pacifci et al. 2015; Kaushal et al. 2023).

There are other parametric SFH models in the literature, such as the delayed τ , log-normal, and double-power law models. Carnall et al. (2019) show that distinguishing between these parametric models using broadband photometry is hard. Since the global shapes of SFHs represented by these models are roughly covered by the two parametric models described above, we only use the Γ and τ models in our study to represent this set of parametric models.

The stepwise model: Non-parametric models are found to be more flexible than parametric models in describing the diversity of SFH shapes. The accuracy of such a model depends on how many time bins are used in the model, which is a trade-off with computational tractability. Using an infinite number of time bins would return the “real” SFH, but it is unrealistic for computational power and time. It is also unnecessary, as real observational data can only constrain a finite number of model parameters. Leja et al. (2019) demonstrate that at least 5 time bins are needed to carry the information from their mock photometric data. Yet, whether non-parametric models may possibly have hidden biases in SFH reconstructions via spectral synthesis modeling is still an open question (Zibetti et al. 2024). Here, we adopt the same model as used in BIGS (Zhou et al. 2020, 2021), which is a slightly modified version of the model developed by Weisz et al. (2011). This model samples the average SFRs in 7 fixed time intervals, specifically:

$$\begin{aligned} & t < 200 \text{ Myr} \\ & 200 < t < 500 \text{ Myr} \\ & 500 \text{ Myr} < t < 1 \text{ Gyr} \\ & 1 < t < 2 \text{ Gyr} \\ & 2 < t < 6 \text{ Gyr} \\ & 6 < t < 10 \text{ Gyr} \\ & 10 \text{ Gyr} < t \end{aligned} \quad (5)$$

For this model, we follow Zhou et al. (2020, 2021) in normalizing the SFH by setting $\text{SFR} = 1$ for the (1 - 2) Gyr bin, and treat the average SFRs in the remaining 6 bins as free parameters. Once the relative heights of the SFRs are determined, the absolute SFRs are scaled up and down together based on the total stellar mass. As a result, the stepwise model contains 6 degrees of freedom.

3.2. Models Based on Principal Component Analysis

3.2.1. Principal Component Analysis

Principal component analysis (PCA) is a commonly used method in data modeling. The general idea behind the PCA is to identify patterns and relationships in high-dimensional data sets and then transform the original correlated high-dimensional coordinates into a set of new, uncorrelated coordinates in directions along which the data have the largest variances. These new coordinates, namely the principal components (PCs), are ranked in order of decreasing variance that the individual PCs account for. Therefore, a PCA on a data set allows us to identify a number of low-order PCs to describe the most significant trends (features) of the entire data set, with higher-order PCs containing information about the details that are either uninteresting to us or cannot be constrained by data.

In astronomy, PCA has been employed in galaxy spectral classification (e.g., Connolly et al. 1995; Yip et al. 2004), identification between quiescent and star-forming galaxies (e.g., Wild et al. 2008), studies of galaxy clustering (e.g., Tegmark & Bromley 1999; Bonoli & Pen 2009; Hamaus et al. 2010; Zhou et al. 2023), the interstellar medium (e.g., Ungerechts et al. 1997; Neufeld et al. 2007; Lo et al. 2009; Melnick et al. 2011; Jones et al. 2012; Gratier et al. 2017), chemical abundances (e.g., Ting et al. 2012) and dark matter halos (e.g., Wong & Taylor 2012; Chen et al. 2020). Here we limit ourselves to a brief description of the PCA, mainly via the singular-value decomposition (SVD) and its application to modeling SFHs. In particular, we adopt the PCA algorithm from scikit-learn (Pedregosa et al. 2011), as described below.

Consider a sample of N_G galaxies, and let the SFH of the i -th galaxy be $f_i(t)$, where $i = 1, 2, \dots, N_G$. We sample the time t in N_t points, t_j , with $j = 1, 2, \dots, N_t$. Thus, the SFH of the i -th galaxy can be considered as a “vector” in the N_t -dimensional hyperspace, $\mathbf{f}_i \equiv [f_i(t_1), f_i(t_2), \dots, f_i(t_{N_t})]$, with $f_i(t_j)$ being the projection of the “vector” along the j -th axis. In practice, we work with the normalized SFH, defined as

$$\hat{f}_i(t_j) = \frac{f_i(t_j)}{\text{mean}(f_i)}, \quad (6)$$

where $\text{mean}(f_i)$ is calculated by the total stellar mass over the age of the universe. To simplify notation, we will omit the hat on \hat{f} and use f to represent the normalized quantity. Thus, the SFH data set of the sample is a $N_G \times N_t$ matrix, A , with each row representing the normalized SFH of one galaxy in the sample.

Fed with the data of a given training sample, the first step of the PCA is to determine an empirical mean vector (of length N_t). This mean vector is used to shift the origin of the original coordinate system to a new point represented by the mean vector. Particularly, the shape of this mean vector is similar to the cosmic star formation rate though not identical because of the limited training sample in our study. Then, the transformation of the old coordinates into the new orthogonal basis is done by a covariance matrix,

$$C(t_k, t_l) \equiv A^T A = \sum_i f_i(t_k) f_i(t_l), \quad (7)$$

which has a dimension of $N_t \times N_t$. The new coordinates, i.e., the eigenvectors (eigen-histories in our study), and eigenvalues are found by performing a singular-value decomposition over the covariance matrix,

$$C = V \Lambda V^T, \quad (8)$$

where the k -th column of V is the k -th eigen-history, denoted by e_k , and Λ is the diagonal matrix containing the eigenvalues, λ_k , that represent the relative importance of each eigenvector. From the PCA construction, the eigenvalues are ranked from high to low, indicating that the first few eigenvectors govern the most dominating features of the training data set. In general, the original data set can be reconstructed using a linear combination of the eigenvectors with the corresponding coefficients, a_k , and the constant mean vector, i.e.,

$$f_i(t_j) = \sum_{k=1}^{N_e} a_{i,k} e_k(t_j) + \text{mean vector}, \quad (9)$$

where N_e is the total number of eigenvectors used in the reconstruction. It is straightforward to see that $N_e = N_t$ if all eigen-histories are used. Since one of our goals is to use only the most important eigen-histories (instead of all of them) to reduce the dimensionality of the SFH representation, we only select the first few eigen-histories based on how much variance they can recover from the original data set. For reference, we examine the PCA-based models when using various numbers of the eigen-histories in Appendix B.

3.2.2. The Development of a PCA-based Model for Star Formation Histories

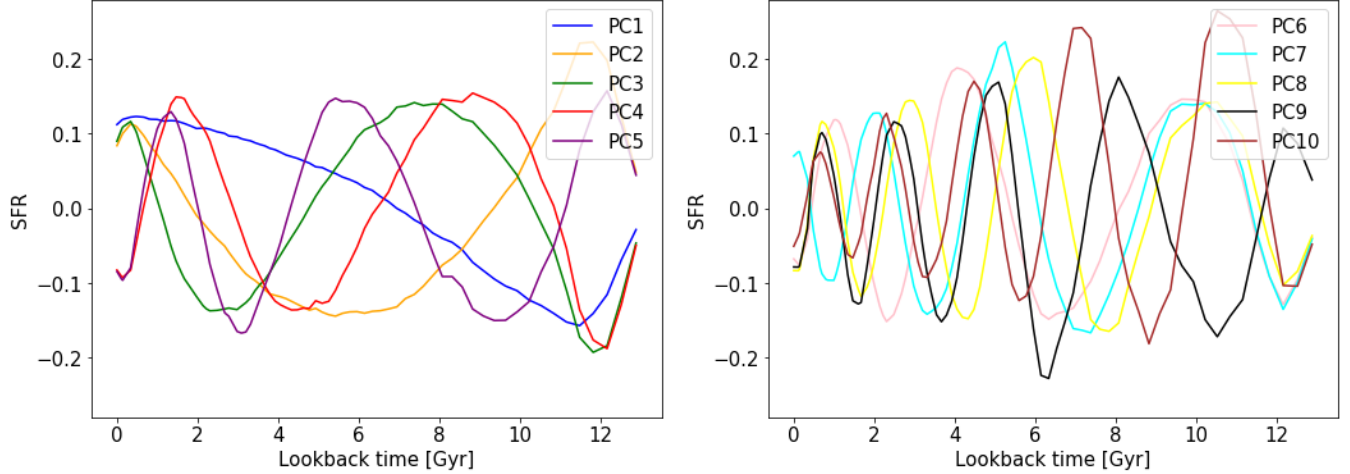


Figure 2. The first 10 eigen-histories of the PCA-based models. The left panel shows lower-order eigen-histories from 1 to 5, and the right panel shows higher-order eigen-histories from 6 to 10. The eigen-histories are sampled in the logarithmic look-back time scale.

As mentioned above, the original TNG100 data, given in redshift, is pre-processed into cosmic time (and look-back time) given the cosmological model adopted. We develop PCA-based models as follows.

The PCA model: Since it is known that galaxy SEDs are light-weighted SFHs, the most recent star formation naturally has a stronger influence on the spectral shape than older stellar populations. We will discuss this effect in more detail later in §4.3. This is also the reason that non-parametric models usually adopt a denser sampling at a later (cosmic) time. We therefore consider a model in which the look-back time, t_{lb} , is re-sampled on a grid of 100 points on a logarithmic scale. By doing so, the most recent SFRs are weighted more importantly relative to the earlier SFRs (see Fig. 1). The first 10 eigen-histories obtained are shown in Fig. 2. As one may see, the eigen-histories oscillate around $SFR = 0.0$, more or less as sinusoidal waves. As the eigen-histories go to higher orders, the oscillation becomes more frequent, indicating that lower-order eigen-histories represent the overall trend of a SFH, while the higher-orders represent the small-scale details. Furthermore, oscillations are more frequent at smaller t_{lb} , especially for higher-order eigen-histories. This arises from the higher weight given to the more recent cosmic time in the PCA model.

We perform a percentage-of-variance-explained (PVE) test on the PCA model. Since the TNG100 training data set is interpolated on a grid of 100 temporal points, there should be 100 independent eigen-histories in total. If all of the eigen-histories are included, the sum of the PVE is 1. In Fig. 3, we plot the cumulative PVE (CPVE) from the first eigen-history to the 15th. Clearly, a small number of the low-order eigen-histories already represent a significant amount of the variance of the data set.

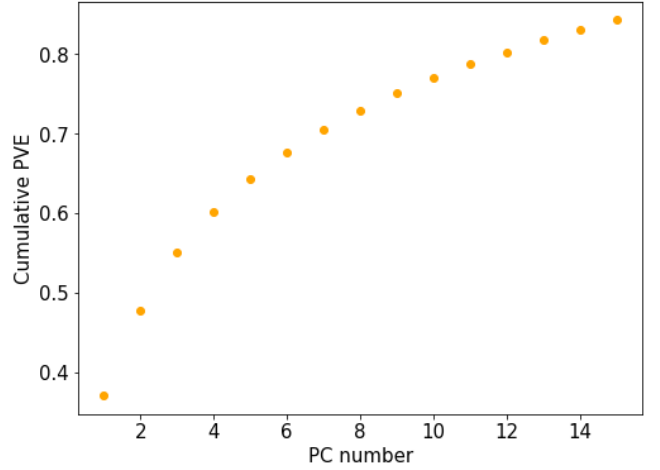


Figure 3. Cumulative percentage of variance explained (CPVE) of the PCA model. The first 5 eigen-histories capture $\sim 65\%$ of the variances in the original TNG100 data.

Although the CPVE value continues to approach 1 as more eigen-histories of higher orders are included, the growth of the CPVE within the first few eigen-histories is faster than that in higher orders. In Appendix B, we statistically study the effect of using different numbers of eigen-histories in the PCA-based models and find that five eigen-histories provide an ideal balance between model simplicity and accuracy in describing the simulated SFHs, while also matching the corresponding mock spectra. Thus, we use five eigen-histories in the PCA-based models throughout the paper unless specified otherwise. As shown in Fig. 3, this choice can capture $\sim 65\%$ of the variance in the original TNG100 data.

The PCA+step model: Owing to the fact that each eigen-history is its own entire history as a function of time, there is a strong entanglement between the old and young stellar populations in the PCA model, and thus also in the composite spectrum. Since a younger population is brighter than an old population of the same total mass, particularly when the stellar age is younger than ~ 1 Gyr, the presence of a recent burst of star formation can affect the spectrum of a galaxy significantly, even if the total amount of stars formed in the burst is small. This can lead to significant bias in the inferences based on the spectrum. To deal with this problem, we modify the PCA Model by including the freedom to tune the SFR in the most recent time interval (a step function). We choose a step that covers 0 - 0.3 Gyr in look-back time based on our tests using different step widths in §4.3. This step adds an extra degree of freedom to the model. Thus, the PCA+step model has the degree of freedom of the PCA model plus 1, which is the same as the stepwise model described above.

4. COMPARISONS BETWEEN MODELS

A successful SFH model should be able to reproduce the diversity of galaxy SFHs. Since the SFH of an observed galaxy is usually inferred from its spectrum, and since the observed spectrum is the light-weighted composite of stellar populations at different ages, another criterion is that the model should not lead to biased inferences of the SFH from the spectrum. Because a SFH model is an approximation to the true SFH, the best fit to the SFH itself does not necessarily mean the best match to the spectrum, and vice versa. It is thus essential to test SFH models in both the SFH space and spectral space. This can be done only for simulated galaxies where SFHs for individual galaxies are available. In this section, we test the representative SFH models described above, alongside the new PCA-based models in both spaces. To this end, we first fit SFHs from the TNG100 to different models and examine their goodness-of-fit. We then compare the spectra generated by each best-fit SFH to the true spectrum generated using the simulated SFH.

4.1. Comparisons in the SFH space

We use the full SFHs of individual galaxies as provided by TNG100, and use a least-squares-fit to fit each SFH (in linear scale) with each of the SFH models described earlier. As mentioned before, we only use data at $z \lesssim 6$. The fitting procedure uses the Python package Non-Linear Least-Square Minimization and Curve-Fitting (LMFIT Newville et al. 2023). Figure 4 shows one example. The left panel shows the best-fit models

in comparison to the original input SFH (grey). As seen from this example, the input SFH has two burst periods, with a major and earlier peak around the look-back time $t_{\text{lb}} \sim 7$ Gyr and a secondary one around $t_{\text{lb}} \sim 1$ Gyr. The Γ model (shown by the dashed blue line) reproduces the earlier peak, but the power-law behavior of the model at lower t_{lb} fails to recover the secondary peak. The τ model (shown by the dashed cyan line) also fails, because it only allows an exponential decay at small t_{lb} . Overall, the two parametric models can roughly recover the general trend of the decreasing SFR with time, but they cannot capture fluctuations in the input SFH. The stepwise model, shown by the brown line, performs reasonably well in capturing the shape of the input SFH at low t_{lb} , but it only provides a coarse approximation at high t_{lb} because of the large steps used.

In contrast, the PCA-based models successfully recover the overall trend, as well as significant higher-order features, such as the two peaks. The two PCA-based models return quite similar least-squares results, as they only differ in the step covering $t_{\text{lb}} = 0 - 0.3$ Gyr. Within the past 0.3 Gyr, the predicted SFR by the PCA model follows a decreasing trend, while adding the step function in the PCA+step model results in better agreement with the SFR in the most recent time bin. As we will show in §4.3, recent star formation carries a large weight in the predicted spectrum. It is thus important to check the performance of SFH models also in the spectral space, as we will do in the next subsection.

Statistically, the success of a model can be quantified by examining its performance on a sample of galaxies covering a variety of SFHs. To this end, we apply the same least square fitting to each of the TNG100 galaxies, and define the following quantity to describe the goodness of match between a model SFH and the original SFH:

$$\Delta_{\text{SFH}} = \frac{\sigma}{\mu} \quad (10)$$

where

$$\mu \equiv \frac{1}{N} \sum_{i=1}^N \text{SFR}_{\text{input},i} \quad (11)$$

is the average SFR over the SFH, and

$$\sigma^2 \equiv \frac{1}{N} \sum_{i=1}^N (\text{SFR}_{\text{input},i} - \text{SFR}_{\text{model},i})^2 \quad (12)$$

is the variance between the input SFH and the best-fit model SFH, with N being the total number of time bins used to represent the SFH. We use $N = 87$ for the TNG galaxies, which corresponds to the snapshots returned directly from the TNG simulation.

The left panel of Fig. 6 shows the probability density distributions of Δ_{SFH} for different models. As one can

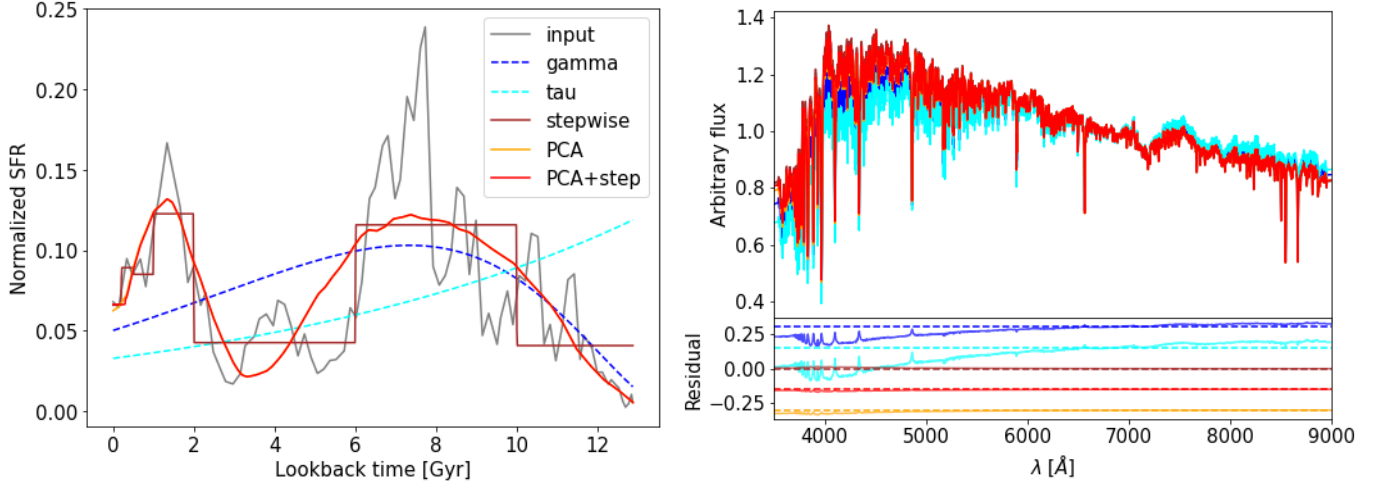


Figure 4. **Left:** An example SFH (gray curve) given by TNG100 and the best fits to it assuming different models. All the SFH curves are normalized to $1 M_{\odot}$. **Right:** Spectrum generated from the original SFH in comparison to those generated from the best-fit SFH models. The spectra are normalized using the mean flux density between 6500 \AA and 7000 \AA . Residuals of the model spectra relative to the spectrum of the input SFH are shown at the bottom of the right panel, with zero-points of the Γ , τ , and PCA-based models shifted by constants.

see, the distributions of Δ_{SFH} for the PCA-based models are similar to each other, peaking at $\Delta_{\text{SFH}} \sim 0.38$. This is expected because these two models differ only by the step covering $t_{\text{lb}} = 0 - 0.3 \text{ Gyr}$. The stepwise model and the Γ model have very similar distributions, both peaking around $\Delta_{\text{SFH}} \sim 0.45$. However, since the degree of freedom of the stepwise model is larger than that of the Γ model, the latter seems quite powerful in modeling the SFH. The PCA+step model has the same degree of freedom as the stepwise model, while the PCA model has one degree less. The fact that their Δ_{SFH} distributions are narrower and have lower mean values suggests that the PCA-based models are more powerful in describing the SFHs of the simulated galaxies used herein. The τ model performs the worst; its Δ_{SFH} distribution is much broader with the largest median Δ_{SFH} value and has a more extended tail towards the large-value end. For reference, we list the values of $\Delta_{\text{SFH}} (\times 10)$ at several percentiles (25, 50, 75, 85, and 95) of the Δ_{SFH} distribution in the first column of Table 1. We note that errors on these percentiles are small, as the distribution functions are well sampled by the data.

As another test of the performance of different SFH models, we calculate the cumulative SFRs of each galaxy in each model and obtain the time, t_f , by which a fraction of $f = 30\%$, 50% , and 70% of the stellar mass has formed, respectively. Fig. 5 shows the deviation (vertical axis) of t_f between a model prediction and that obtained from the input SFH, with the horizontal axis plotting the corresponding t_f of the input SFH. Results are shown for different models, as indicated on the top of the plot, and for the three percentiles, as indicated

on the right-hand side. The light points are the results of individual galaxies, while the black points connected by thick lines are the median values estimated in 6 formation time bins, with error bars indicating the 5-95 percentile range. A positive (negative) value of the deviation implies that the SFH model predicts a later (an earlier) time to form the given fraction of stellar mass than the input SFH.

As seen from Figure 5, the τ model shows significant systematic deviations from the ground truth in each mass fraction. For galaxies that have a given fraction of their stars formed early (late) according to the input SFH, the τ model tends to predict a later (earlier) formation time. The performance of the Γ model is much better, even though it has the same degrees of freedom as the τ model. The median of each time bin given by the Γ model is quite close to zero (indicated by the gray dashed line) with error bars much smaller than those given by the τ model. We notice that, for the formation time of the 70% mass, the predicted formation time tends to be slightly later than the input values for times earlier than $\sim 5 \text{ Gyr}$, indicating that the Γ model does not perform ideally for galaxies that have a significant amount of old stars. For the stepwise model, the overall deviation from the ground truth is small. For all of the mass formation times, this model predicts a slightly earlier formation time than the input values. The two PCA-based models have similar performances, with the predicted medians all close to zero. The scatters represented by the error bars are also quite small, typically about $0.1 - 0.5 \text{ Gyr}$ and independent of the formation time. All in all, the results shown in Fig. 5 demonstrate

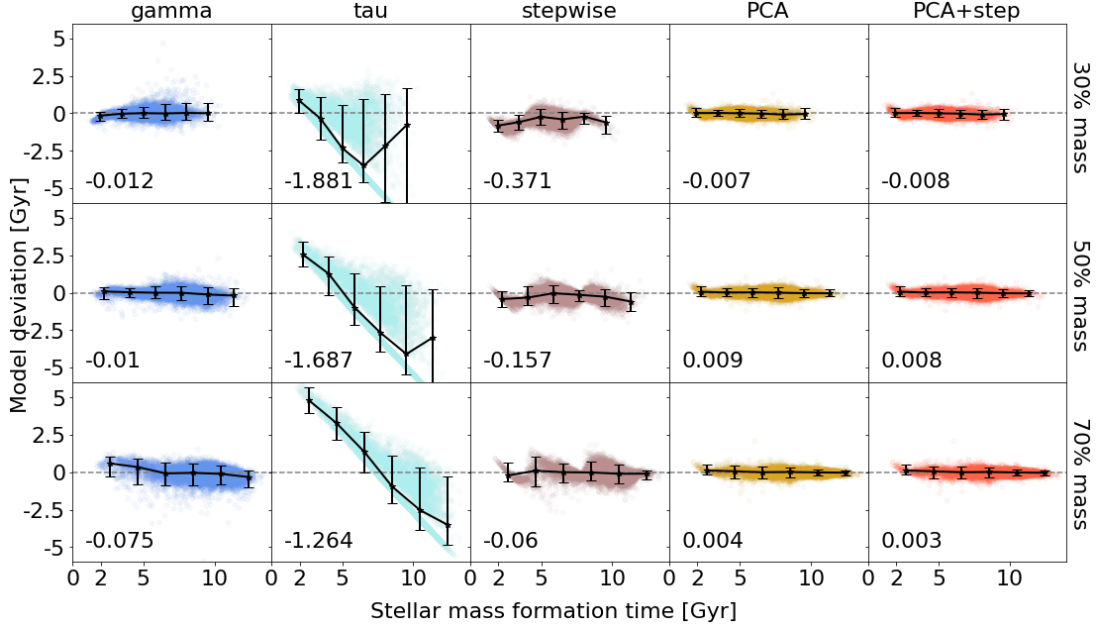


Figure 5. Comparing fractions of mass formation time from each SFH model to the ground truth (marked by the gray dashed line). The x-axis marks the mass percentage formation time, and the y-axis is the time deviation between the model prediction and that obtained from the input SFH. Each SFH model is indicated by the column title, and each row represents 30%, 50%, and 70% of the total stellar mass formed. In each panel, the light color dots represent individual simulated galaxies in the sample. We bin the real formation time in 6 time bins and mark the median deviation using the black dots. The error bars indicate 5 and 95 percentiles from the bins. Furthermore, the median value of model deviation from the entire data set is labeled at the lower left corner of each panel.

that the PCA-based models can provide an accurate representation of the simulated SFHs.

4.2. Comparisons in the spectral space

Since the observed spectrum of a galaxy is its SFH weighted by the light of stellar populations of different ages, we need to check if the predicted spectrum of a best-fit SFH model can also match the spectrum expected from the original input SFH. To test this, we generate mock spectra using the best-fit SFHs and compare them to the spectra generated using the input SFHs. To isolate the effects produced by SFH, we keep all other factors (IMF, dust, metallicity, etc.) the same. All the spectra are generated for the full wavelength range of 3500 - 9000 Å and normalized using the mean flux between 6500 - 7000 Å. An example, generated using the SFHs shown in the left panel, is shown in the right panel of Fig. 4. From the residual plot, we see that the spectra generated by both the τ and Γ models significantly underestimate the input spectrum in the blue end, clearly because these two models miss the secondary peak in the SFH at low t_{lb} . The stepwise model and the two PCA-based models have a similar performance in matching the input spectrum, showing no significant offset from zero in the residual. These results demonstrate that, for some cases such as the one shown here, the performance

of a model in the spectral space can be quite different from that in the SFH space. The difference in the spectra between the PCA model and PCA+step model is almost entirely produced by the small difference of the SFH in the most recent time bin, $t_{\text{lb}} = 0 - 0.3$ Gyr, indicating that it is important to take into account recent star formation in a SFH model to obtain unbiased inferences of the SFH from the synthesized spectrum.

We calculate the Δ_{spec} value of each model spectrum relative to the input mock spectrum for the full spectral coverage using the same equation as shown in Eq. 10 but for the flux density instead of the SFR, and obtain the probability distribution of Δ_{spec} predicted by each of the SFH models for the TNG sample. The percentiles of the distributions are summarized in the second column of Table 1 for each model. It is seen that both the τ and Γ models have the largest percentile values, indicating a poor performance of these two models in the spectral space. The percentile values of the PCA model are about four to six times as large as those of the PCA+step model, indicating again the importance of correctly modeling the recent star formation in a SFH model. The stepwise model ranks next to the PCA+step model, with similar statistics in Δ_{spec} , although its performance in the SFH space is worse.

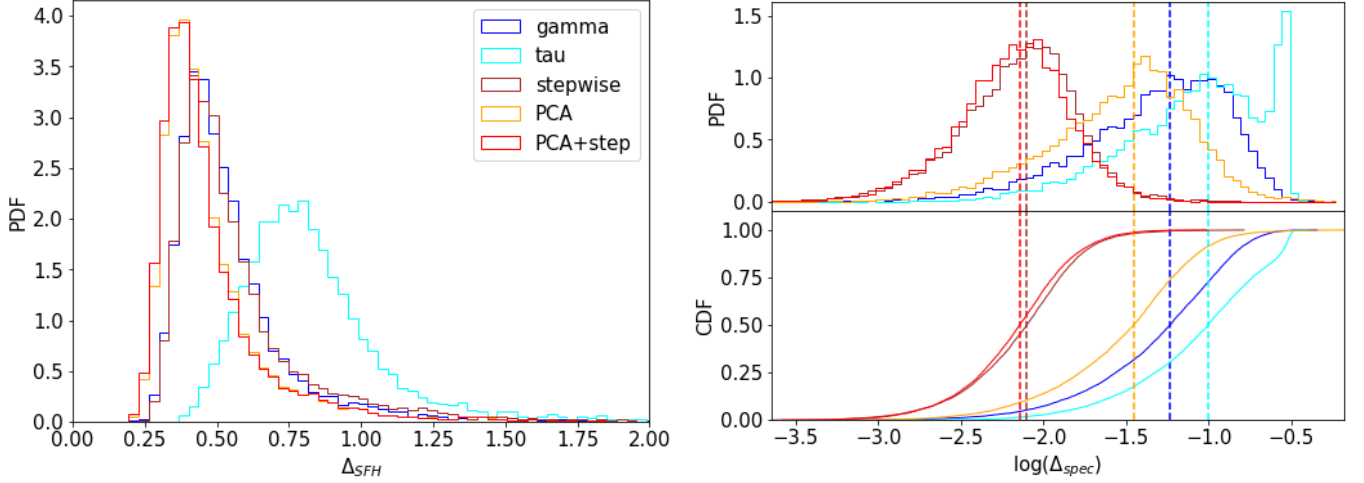


Figure 6. **Left:** Probability density distribution of Δ_{SFH} . The PCA-based models share similar distributions with a peak at $\Delta_{\text{SFH}} \sim 0.38$, the smallest compared to all the other models. The Γ model and stepwise model share similar distributions, both peak at $\Delta_{\text{SFH}} \sim 0.45$, while the τ model has the largest peak value of ~ 0.75 . **Right:** The upper panel is the probability density distribution in $\log(\Delta_{\text{spec}})$ bin, and the lower panel is the corresponding cumulative distribution. The dashed lines mark the median Δ_{spec} value of each model. Models use the same color codes as in the LHS panel.

Model	$\Delta_{\text{SFH}} \times 10$	$\Delta_{\text{spec}} \times 100$	Sample
	25% - 50% - 75% - 85% - 95%	25% - 50% - 75% - 85% - 95%	
Γ	4.2 - 4.9 - 6.1 - 7.0 - 9.9	2.7 - 5.8 - 10.5 - 13.3 - 18.6	TNG100 central
	(4.8 - 6.0 - 8.3 - 10.8 - 23.0)	(2.7 - 6.0 - 11.6 - 15.3 - 22.6)	TNG100 satellite
	[2.6 - 3.1 - 3.9 - 4.5 - 6.4]	[2.3 - 4.9 - 8.8 - 11.3 - 15.7]	EAGLE central
τ	6.7 - 7.9 - 9.3 - 10.3 - 13.3	4.7 - 9.9 - 18.4 - 25.7 - 30.3	
	(7.3 - 8.9 - 11.6 - 14.3 - 26.2)	(8.5 - 20.1 - 29.3 - 30.7 - 32.4)	
	[5.6 - 6.4 - 8.0 - 8.8 - 10.8]	[3.3 - 7.3 - 13.9 - 19.9 - 27.6]	
Stepwise	4.2 - 5.0 - 6.3 - 7.6 - 11.1	0.4 - 0.8 - 1.3 - 1.6 - 2.4	
	(4.9 - 6.5 - 9.4 - 11.9 - 18.6)	(0.5 - 0.9 - 1.4 - 1.8 - 3.5)	
	[3.2 - 3.9 - 4.9 - 5.8 - 8.3]	[0.3 - 0.6 - 1.0 - 1.6 - 3.5]	
PCA	3.6 - 4.2 - 5.3 - 6.2 - 8.9	1.7 - 3.5 - 6.0 - 7.9 - 12.0	
	(4.1 - 5.3 - 7.4 - 9.6 - 20.0)	(2.3 - 5.0 - 9.4 - 12.8 - 20.8)	
	[2.2 - 2.7 - 3.4 - 3.9 - 5.8]	[0.8 - 1.8 - 3.3 - 4.4 - 8.5]	
PCA+step	3.5 - 4.2 - 5.2 - 6.2 - 8.9	0.4 - 0.7 - 1.1 - 1.5 - 2.3	
	(4.1 - 5.2 - 7.4 - 9.5 - 17.7)	(0.5 - 0.8 - 1.5 - 2.0 - 3.7)	
	[2.2 - 2.7 - 3.4 - 3.9 - 5.8]	[0.2 - 0.4 - 0.7 - 0.9 - 1.3]	

Table 1. Percentiles of Δ_{SFH} and Δ_{spec} statistics for TNG100 central galaxies in the SFH (the first column) and spectral (the second column) spaces. The five values from left to right in each unit are the 25% - 50% - 75% - 85% - 95% percentiles. The values in the parenthesis are from TNG100 satellite galaxies, and the values in the square brackets are from EAGLE central galaxies.

The right panel of Fig. 6 shows the full distribution of Δ_{spec} for each model. The distribution obtained from the τ model extends to very large values, as seen from the slowly-growing cumulative distribution. The Γ model performs slightly better than the τ model, but again with a large Δ_{spec} at the peak and a slowly-growing cumulative distribution. These results suggest that these parametric models cannot reproduce

the spectra of many simulated galaxies. The stepwise model has much better statistics, as can be seen from the higher probability at the lower Δ_{spec} end, as well as the relatively fast growth of the cumulative distribution. Roughly 50% of the galaxies in our sample have a Δ_{spec} smaller than ~ 0.008 in the stepwise model, in comparison to ~ 0.1 for the τ model and ~ 0.06 for the Γ model. For PCA-based models, we can see

the significant improvement from the PCA model to the PCA+step model, with the Δ_{spec} distribution shifting from large to small values and the cumulative distribution becoming successively steeper. The PCA+step model returns the best statistics among all models: the median Δ_{spec} is ~ 0.007 , slightly smaller than that of the stepwise model, ~ 0.008 . And more than 55% of the galaxies have their Δ_{spec} values lower than 0.008. Overall, the stepwise model and PCA+step model perform the best in the spectral space, although the stepwise model is less accurate in the SFH space (see §4.1).

In addition, we test the Δ_{spec} behavior at various wavelength coverages, e.g., 4MOST blue and green bands (de Jong et al. 2019), PFS blue and red bands (Takada et al. 2014), and various narrow bands, and find that the stepwise and PCA+step models always result in the best statistical behavior comparing to the other SFH models, with more significant improvements in the bluer bands. This is consistent with what is shown in the right panel of Fig. 4, where the spectral residual shows the strongest wavelength dependency at the blue end. This also indicates a strong influence on a galaxy spectrum from the youngest stellar population, in agreement with §4.3.

Comparing the statistics in Δ_{SFH} and Δ_{spec} , one sees that the median values in the SFH space are generally an order of magnitude larger than those in the spectral space, as shown in Table 1. This demonstrates that differences in the SFH space are significantly smeared out in the spectral space. Such a “smearing effect” makes it difficult to constrain the SFH of a galaxy from its spectrum, and indicates that it is crucial to design SFH models carefully to obtain unbiased inferences of SFH from synthesized spectra. As pointed out above, this requires a SFH model that performs consistently in both the SFH and spectral spaces. Based on the results presented above, we find that the PCA+step model performs consistently in both spaces. In what follows, we perform further tests of this model in comparison with traditional models.

4.3. Impacts of most recent star formation

As shown in Fig. 4, some of the best-fit SFHs produce spectra that are quite different from those of other SFH models. Since all other factors are kept the same except the shape of the SFH curve, it raises the question of what part of the SFH causes this discrepancy, and how significant the effect can be. For the example shown in Fig. 4, the most noticeable difference from the best-fit SFHs is the most recent SFR, where the two parametric models have noticeably lower SFRs compared to the stepwise model and the PCA-based models. The

dramatically different behavior between the PCA model and the PCA+step model in the spectral space, shown in Fig. 6, reveals the same problem. Since the two PCA-based models only differ by the step function at $t_{\text{lb}} = 0 - 0.3$ Gyr, the difference indicates the importance of including the freedom to account for the most recent star formation. The choice of the step width, 0-0.3 Gyr, is not justified *a priori*. Here, we test the influence of different step widths, specifically from 0.1 Gyr to 0.5 Gyr.

We repeat the same Δ_{SFH} and Δ_{spec} tests as we did in previous sections. As shown in the left panel of Fig. 7, the distribution of Δ_{SFH} is almost independent of the step width, as expected from the fact that the amount of star formation in the most recent time step is small in comparison to the entire SFH. Thus, from the SFH perspective, all of these step widths are equally valid. However, when the best-fit SFHs are used to generate model spectra, it seems that a width of 0.3 Gyr is preferred, as shown in the right panel of Fig. 7. The next best width is 0.2 Gyr, then 0.1 and 0.4 Gyr, of which the distributions of Δ_{spec} have similar median values, but slightly larger than that of the best choice. As the step width increases to 0.5 Gyr, the peak of the distribution is shifted towards larger Δ_{spec} , and the median is about 2 to 3 times as large as that of the best choice. These test results show that the choice of 0.3 Gyr for the step width is close to optimal.

4.4. Effects of adding noise

The input mock spectrum shown in Fig. 6 contains no noise. However, measured signals always come with noise in real observations. Therefore, we test the acceptability of the selected SFH models at various signal-to-noise ratios (SNR). To this end, we add Gaussian noise with zero mean and a standard deviation σ_{noise} to the input mock spectra, thus generating spectra with $\text{SNR} = 1/\sigma_{\text{noise}}$ per Angstrom. We vary the SNR from 2 to 40 (and 100 for the comparison between the stepwise and PCA+step models) and calculate the reduced chi-square in the predicted spectrum for each SFH model relative to the ground truth. The χ^2_{ν} is calculated using

$$\chi^2_{\nu}(\text{SNR}) = \frac{1}{N-1} \sum_i^N \frac{(f_{\text{input},i} - f_{\text{model},i})^2}{\sigma_{\text{noise}}^2}, \quad (13)$$

and is shown in the top panel of Fig. 8. We plot the 50 percentiles using solid lines and the 25 and 75 percentiles using error bars. For reference, we also show the spectrum of the galaxy shown in Fig. 4 with noise at $\text{SNR} = 2$ and $\text{SNR} = 40$ in comparison to the spectra given by different SFH models.

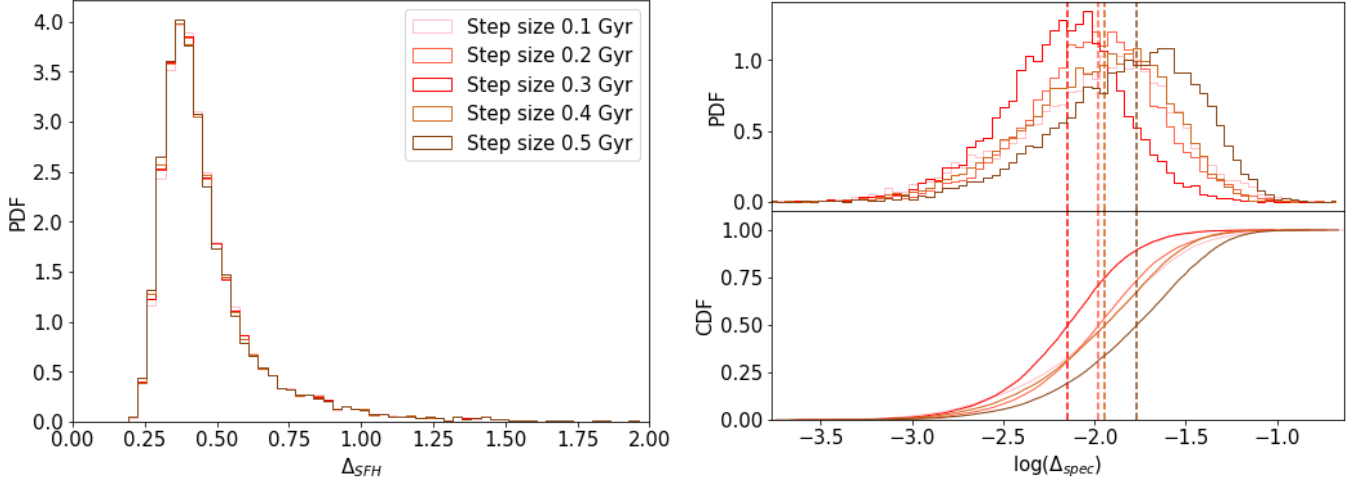


Figure 7. Probability density distributions of Δ for the PCA+step model with various step sizes (0.1 to 0.5 Gyr) in the SFH space (left panel) and the spectral space (right panel). The 0.3 Gyr step size model (plotted in red) is the PCA+step model shown in the previous plots.

Using the best-fit SFH, the χ^2_ν of the Γ and τ models decreases rapidly with the SNR. This can be understood by comparing the spectral plots in Figs. 4 and 8. When the predicted spectra are compared with the noise-free input spectrum in Fig. 4, the best-fit SFHs of the Γ and τ models perform poorly in the spectral space. At SNR = 40, the discrepancies of these models at the short-wavelength end with the zero-points defined by the ground truth are still very significant. However, as the input mock spectrum becomes highly noisy, e.g. at the SNR = 2 level, all of the SFH models are “acceptable” in the spectral space. As one can see from the top panel showing χ^2_ν as a function of the SNR, a moderate SNR is required to reject the τ and Γ models, but a very high SNR is needed to reject the stepwise model and the PCA+step model. This demonstrates that the inference of the SFH from a noisy spectrum can be biased by using a restrictive model for the SFH, such as the parametric models.

It is interesting to see that the PCA model, which is flexible enough in describing the overall SFH and can accurately predict the formation times of fixed fractions of stellar mass (Fig. 5), does not perform as well as the PCA+step model in the spectral space. As shown in Fig. 8, the growth rate with increasing SNR of the PCA model is the next fastest besides the two parametric models. About 50% of the model spectra can be rejected (using $\chi^2_\nu > 1$ to indicate a significant discrepancy) at SNR = 3 - 5, and 75% can be rejected at SNR = 5 - 10. In contrast, the PCA+step model makes a large improvement in the spectral space: it has 50% of the spectra rejected at SNR = 5 - 10 and 75% at SNR = 40.

Comparing the stepwise model and the PCA+step model, one sees that the PCA+step model is slightly favored starting from SNR = 20 to higher SNRs. Overall, these two models have a similar performance in the spectral space, even in the presence of noise.

5. THE APPLICABILITY OF PCA-BASED MODELS

So far, we have demonstrated the validity of the PCA-based models using the same data set as used for the model training (i.e., to obtain the eigen-histories). Yet, it is important to test the validity of the models using different populations of galaxies. In this section, we first test models using central galaxies in three stellar mass bins in the TNG100 simulation (§5.1). We then test in §5.2 the validity of the models on TNG100 satellite galaxies that are not used in training the PCA-based models. Finally, in §5.3, we test models using central galaxies selected from the EAGLE simulation.

5.1. Tests on different stellar mass bins

To this end, we divide the selected central galaxies from the TNG100 sample into 3 mass bins: low-mass ($M_* < 10^{10} h^{-1} M_\odot$), intermediate-mass ($10^{10} h^{-1} M_\odot \leq M_* < 5 \times 10^{10} h^{-1} M_\odot$), and high-mass ($M_* > 5 \times 10^{10} h^{-1} M_\odot$), and run the Δ_{SFH} and Δ_{spsc} tests for each subsample. The results for the SFH space and the spectral space are shown in the left and right panels of Fig. 9, respectively.

In the SFH space, the τ model performs the worst in all mass bins. The performances of the Γ and stepwise models are comparable in each mass bin, although the latter performs slightly poorer for high-mass and intermediate-mass galaxies. This may be a result of the

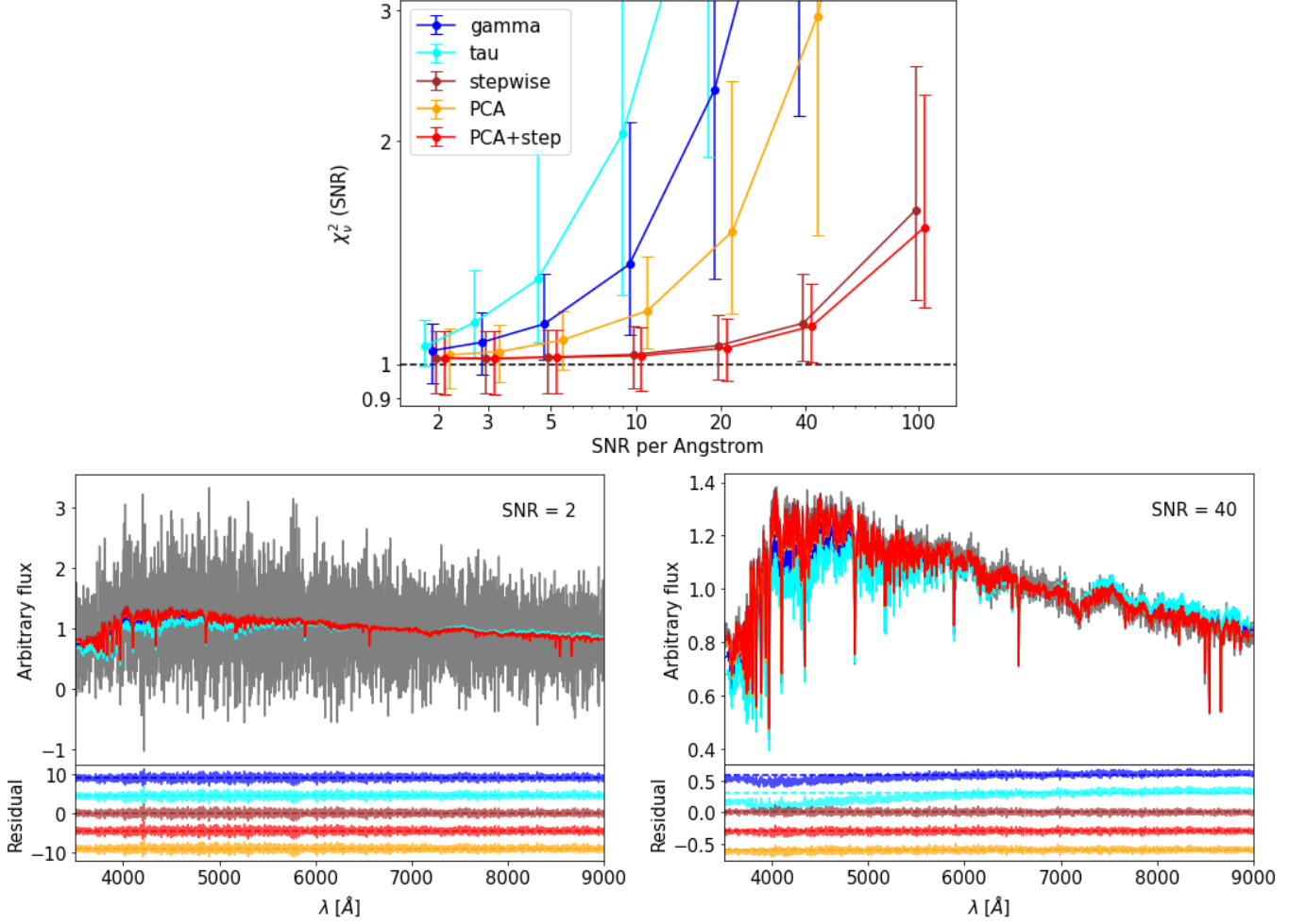


Figure 8. Top: The χ^2_v statistics of TNG100 galaxy spectral comparison at various signal-to-noise ratios (per wavelength). The spectra are generated using the best-fit SFHs of the Γ model (blue), τ model (cyan), stepwise model (brown), PCA model (orange), and PCA+step model (red). The solid lines mark the 50 percentile of each model, while the error bars mark the 25 and 75 percentiles. We shift each model curve horizontally so that the percentile markers can be clearly seen at each SNR. **Bottom:** The same galaxy spectral comparison as shown in Fig. 4 at SNR = 2 and SNR = 40 levels. The zero-points of each residual are shifted up or down by constants.

original design of the stepwise model since more massive galaxies tend to form their stars earlier while the stepwise model puts more weight on later star formation in a galaxy. Overall, the two PCA-based models have the lowest median of Δ_{SFH} in each mass bin. There is a common trend in the PCA-based models for different mass bins: the median of Δ_{SFH} is the smallest for the low-mass sample and the largest for the high-mass sample. This is expected from the design of the PCA-based models: more than 70% of the TNG100 galaxies are categorized as low-mass galaxies, while less than 5% of the galaxies are categorized as high-mass. The training sample we used to obtain the eigen-histories is therefore dominated by low-mass galaxies and thus features in their SFHs are better represented. However, such a trend is also seen in the traditional models that are

not influenced by the training process. This indicates that low-mass galaxies in the TNG simulation on average have simpler SFHs than higher-mass galaxies. It is also interesting to note that the performance ranking of a particular model does not change significantly between the three mass samples, indicating that the diversity in the SFH depends systematically on galaxy mass.

The Δ_{spec} statistics are quite different from those in the SFH space. For the Γ model, the smallest median value of Δ_{spec} comes from the high-mass sample, while the largest median comes from low-mass galaxies. In contrast, for the τ model, the largest median Δ_{spec} comes from high-mass galaxies. Overall, the median Δ_{spec} values of the two parametric models are the largest among all models. Remarkably, for the stepwise model, the median Δ_{spec} values of different mass

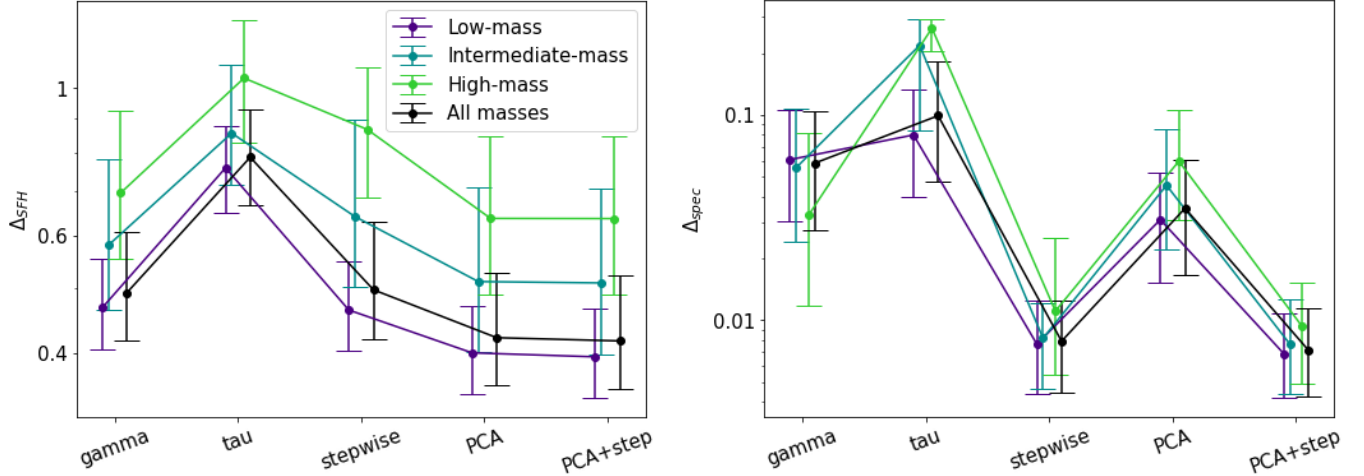


Figure 9. The median Δ values of each SFH model in the low-mass ($M_* < 10^{10} h^{-1} M_\odot$), intermediate-mass ($10^{10} h^{-1} M_\odot \leq M_* < 5 \times 10^{10} h^{-1} M_\odot$), and high-mass ($M_* > 5 \times 10^{10} h^{-1} M_\odot$) bins in the SFH space (LHS panel) and in the spectral space (RHS panel). The Δ statistic for all-mass galaxies is also shown in the figures as the black curve for reference. The upper and lower error bars mark the 25 and 75 percentiles of the distributions.

bins are all similar to each other, suggesting that this model works equally well for different galaxy masses in the spectral space. This indicates again that the early star formation, which may depend systematically on stellar mass, has little influence on the spectrum. Furthermore, the stepwise model reproduces the input mock spectra quite well, as indicated by the small values of Δ_{spec} for all mass bins. The improvement of the PCA+step model over the PCA model is significant and similar for all mass bins in the spectral space, although the statistics of the two models are very similar in the SFH space. This suggests that the most recent star formation (within ~ 0.3 Gyr) plays an important role in the spectral space for galaxies of different masses. Finally, the median Δ_{spec} values predicted by the PCA+step model are slightly smaller than those by the stepwise model in all mass bins, indicating that the improvement made by PCA+step is independent of galaxy mass.

5.2. Test on satellite galaxies

The star formation of satellite galaxies may be affected by environmental processes that are not significant for central galaxies, such that the SFHs of satellites may be systematically different from those of centrals. It is thus important to use satellite galaxies to test the validity of the PCA-based models that are trained by central galaxies. To this end, we select from TNG100 satellite galaxies at $z = 0$ with stellar masses above $1.0 \times 10^9 h^{-1} M_\odot$. This gives a total of 6,852 satellites.

The same Δ analyses as described in §4.1 and §4.2 are carried out for the TNG100 satellite galaxies, and the results are shown by the blue lines in Fig. 10 and Table 1. Similarly to the previous tests based on TNG100 central

galaxies, the performance of the Γ and stepwise models in the SFH space are similar, the τ model is the worst, while the two PCA-based models perform equally and the best. As one can see from Table 1, the percentile values of Δ_{SFH} predicted by the PCA-based models for satellite galaxies are all higher than for central galaxies. This can be understood since the training data comes from TNG100 central galaxies only. However, the same pattern is also seen in the traditional SFH models, indicating that environmental effects on satellite galaxies make their SFHs more diverse.

In the spectral space, the Δ_{spec} values plotted in the right panel of Fig. 10 and listed in Table 1 show that the performance of the τ model becomes significantly worse for satellite galaxies, while for all other models, the performance for satellites is only slightly worse than for centrals. This is in contrast to the performance in the SFH space, where all models become apparently worse for satellite galaxies. This indicates again the nonlinear correlation and degeneracy of SFHs in the spectral space. All in all, the PCA-based modeling, typically the PCA+step model, is still preferred by satellite galaxies in the TNG100 simulation.

5.3. Test on EAGLE galaxies

We further test the robustness and flexibility of the new PCA-based models using the EAGLE simulation (Schaye et al. 2014; Crain et al. 2015), which is another cosmological hydrodynamics simulation running on a modified version of the N-body Tree-PM smoothed particle hydrodynamics (SPH) code (Springel 2005). We use L100N1504, which simulates galaxy evolution from $z = 20$ to $z = 0$ in a cubic box of side length $L_{\text{box}} \sim$

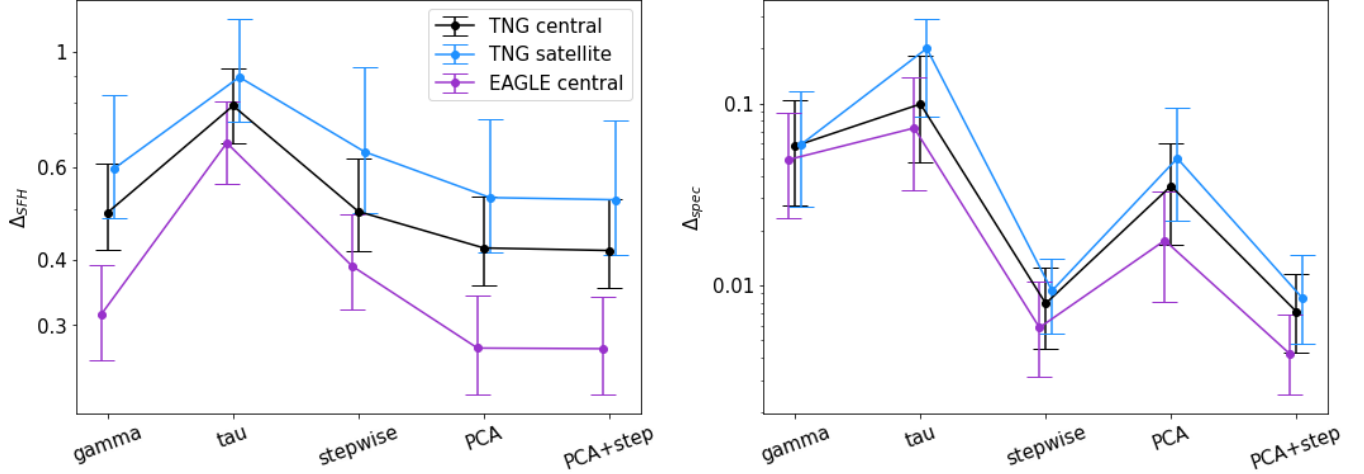


Figure 10. Δ statistics in comparing different simulated galaxy populations, i.e., TNG100 centrals, TNG100 satellites, and EAGLE centrals, in the SFH (LHS) and spectral (RHS) spaces. The dots mark the 50 percentile values, and the error bars mark the 25 and 75 percentile values.

100 cMpc with a mass resolution, $m_{\text{gas}} \sim 1.81 \times 10^6 M_{\odot}$. The cosmology model adopted in EAGLE is the Planck 2013 results (Planck Collaboration et al. 2014).

Out of the 10,860 galaxies with stellar mass $M_{*} \geq 1 \times 10^9 h^{-1} M_{\odot}$ at $z = 0$, we select only central galaxies, which gives a total of 6,160 galaxies. Again, we only use snapshots at $z \lesssim 6$. The total number of snapshots is 23 in the EAGLE simulation, much smaller than the 87 used for the TNG100. To make a more faithful comparison between the two simulations, we first interpolate the EAGLE data onto the TNG snapshots. To mimic the short time-scale fluctuations that are not captured by EAGLE due to its lower temporal resolution, we add random fluctuations using a log-normal distribution obtained from TNG100 central galaxies at individual snapshots. Specifically, the log-normal distributions at different snapshots are obtained by modeling the differences between the original SFHs of individual TNG100 central galaxies with the corresponding smoothed SFHs, obtained from interpolating the original TNG100 SFHs onto the EAGLE sampling and then interpolating back to the TNG100 sampling.

Using the same methodology as for TNG100 galaxies, we study the Δ statistics in both the SFH and spectral spaces. The results are shown in both Fig. 10 and Table 1. Overall, the performance of different models for EAGLE galaxies is similar to those for TNG100. For a given model, the value of Δ_{SFH} for EAGLE tends to be smaller than that for TNG100. This is because the original time resolution of EAGLE snapshots is lower than TNG100, so that the SFHs of EAGLE galaxies are smoothed relative to those of TNG galaxies when we interpolate the EAGLE data onto the TNG resolution. The short time-scale fluctuations we added to the

interpolated EAGLE SFHs are assumed to be random, which may underestimate Δ_{SFH} . In the spectral space, the performances of different models are very similar between EAGLE and TNG100. In particular, the two PCA-based models perform well for EAGLE galaxies, giving more support to the validity of the TNG-trained eigen-histories in modeling the SFHs of galaxies.

6. SUMMARY AND DISCUSSION

In this paper, we examine the statistical behavior of some commonly used star formation history (SFH) models (the Γ , τ , and stepwise models) in fitting simulated SFHs (the SFH space) and compare their synthesized spectra to the “ground-truth” (input) spectra (the spectral space). Meanwhile, we develop a new, generic SFH model using principal component analysis (the PCA-based model), trained by central galaxies selected from the state-of-the-art cosmological hydrodynamic simulation IllustrisTNG. The key results are summarized as follows.

For the development of the PCA-based models, we obtain eigen-histories (the principal components). According to the percentage of variance explained (PVE) test (Fig. 3), the PCA-based models can explain $\sim 65\%$ of the data variance by using the first 5 eigen-histories. We suggest that this choice is optimal in order to balance model simplicity and accuracy (see Appendix B).

To test the flexibility of the SFH models, we use a least-square fitting methodology to fit the SFH models to the input SFHs given by TNG100. Statistically, we define a goodness-of-fit metric Δ_{SFH} to represent the overall deviation of the best-fit models from the input SFHs. We find that the PCA-based models fit the simulated SFHs the best, followed by the Γ and stepwise

models, with the τ model being the least flexible (Fig. 6). The same conclusion is also reached by comparing the simulated and predicted formation time by which a fixed fraction of the total stellar mass is formed in a galaxy (Fig. 5).

Using the best-fit SFHs and the input SFHs, we generate synthesized mock spectra and compare between them. We again use a goodness-of-fit metric, Δ_{spec} , to characterize model performances in a statistical manner. We find that the stepwise and PCA+step models match the input mock spectra well, while the other models do not have the flexibility to cover the diversity in the spectral space (Fig. 6). We find that the most recent star formation activity significantly impacts the spectral shape, which can be modeled well by including in the SFH a step in age between 0 to 0.3 Gyr (Fig. 7). We also examine the effects of adding random Gaussian noise to the input mock spectra to mimic observational data. We find that high signal-to-noise spectra (at least $\text{SNR} > 20$) are required to distinguish the stepwise and PCA+step models that perform the best in the spectral space (Fig. 8).

We test different SFH models by applying them to different galaxy populations (Fig. 10). We find similar model behaviors in both the SFH and spectral spaces for different populations of galaxies, indicating that our test results are valid without depending on the galaxy population in question.

Comparing the model behaviors in the SFH and spectral spaces, we notice that the performance of a given model in these two spaces may differ significantly. This demonstrates the nonlinear connection between a SFH and the associated spectrum, suggesting that the performance of a model should be tested in both spaces and that a careful choice of the SFH model is needed to infer the SFH from the observed spectrum through spectral synthesis modeling.

Overall, the PCA-based models are the most flexible in the SFH space. In particular, the PCA+step model also reproduces the input mock spectra the best. Whereas the PCA+step model has a similar performance in the spectral space as the stepwise model, it performs significantly better in the SFH space. The flexibility and accuracy of the PCA+step model thus make it a promising SFH model candidate in spectral synthesis modeling. So far, we have tested the PCA-based models only from the theoretical perspective. In the near future, we plan to apply the new model to SED fitting. Using BIGS, we will be able to estimate the entire posterior probability distributions of SFH parameters, as well as to explore the degeneracy in the inferred SFH. In addition, allowing the dust and metallicity parameters to vary in spectral synthesis modeling can give us more insight into the age-dust-metallicity degeneracy with the new SFH model. We also plan to apply the new PCA-based model to high-redshift galaxies, especially with the data provided by the James Webb Space Telescope, where the limited data generally requires more careful modeling. Finally, the physically motivated eigenhistories naturally lead to a corresponding ‘PC-spectra’ as an alternative template for spectral synthesis modeling. We intend to compare the new template with the state-of-the-art SSM codes, such as EAZY (Brammer et al. 2008) and pPXF (Cappellari 2017).

1 We gratefully acknowledge Dr. Yangyao Chen for his
2 help in data analysis and detailed explanations. The
3 authors also want to thank Dr. Kai Wang for the in-
4 sightful discussion.

5 *Software:* NUMPY (Harris et al. 2020), SCIPY (Vir-
6 tanen et al. 2020), MATPLOTLIB (Hunter 2007), PANDAS
7 (pandas development team 2024), LMFIT (Newville et al.
8 2023), SKLEARN (Pedregosa et al. 2011), H5PY (Collette
9 et al. 2023).

REFERENCES

- Behroozi, P. S., Wechsler, R. H., & Conroy, C. 2013, *ApJ*, 770, 57, doi: [10.1088/0004-637X/770/1/57](https://doi.org/10.1088/0004-637X/770/1/57)
- Bertelli, G., Bressan, A., Chiosi, C., Fagotto, F., & Nasi, E. 1994, *A&AS*, 106, 275
- Bonoli, S., & Pen, U. L. 2009, *Monthly Notices of the Royal Astronomical Society*, 396, 1610, doi: [10.1111/j.1365-2966.2009.14829.x](https://doi.org/10.1111/j.1365-2966.2009.14829.x)
- Brammer, G. B., van Dokkum, P. G., & Coppi, P. 2008, *ApJ*, 686, 1503, doi: [10.1086/591786](https://doi.org/10.1086/591786)
- Bruzual, G., & Charlot, S. 2003, *Monthly Notices of the Royal Astronomical Society*, 344, 1000, doi: [10.1046/j.1365-8711.2003.06897.x](https://doi.org/10.1046/j.1365-8711.2003.06897.x)
- Calzetti, D., Armus, L., Bohlin, R. C., et al. 2000, *The Astrophysical Journal*, 533, 682, doi: [10.1086/308692](https://doi.org/10.1086/308692)
- Cappellari, M. 2017, *MNRAS*, 466, 798, doi: [10.1093/mnras/stw3020](https://doi.org/10.1093/mnras/stw3020)
- Carnall, A. C., Leja, J., Johnson, B. D., et al. 2019, *ApJ*, 873, 44, doi: [10.3847/1538-4357/ab04a2](https://doi.org/10.3847/1538-4357/ab04a2)
- Carnall, A. C., McLure, R. J., Dunlop, J. S., & Davé, R. 2018, *MNRAS*, 480, 4379, doi: [10.1093/mnras/sty2169](https://doi.org/10.1093/mnras/sty2169)

- Chabrier, G. 2003, *Publications of the Astronomical Society of the Pacific*, 115, 763, doi: [10.1086/376392](https://doi.org/10.1086/376392)
- Chen, Y., Mo, H. J., Li, C., et al. 2020, *ApJ*, 899, 81, doi: [10.3847/1538-4357/aba597](https://doi.org/10.3847/1538-4357/aba597)
- Collette, A., Kluyver, T., Caswell, T. A., et al. 2023, *h5py/h5py: 3.8.0-aarch64-wheels, 3.8.0-aarch64-wheels*, Zenodo, doi: [10.5281/zenodo.7568214](https://doi.org/10.5281/zenodo.7568214)
- Connolly, A. J., Szalay, A. S., Bershad, M. A., Kinney, A. L., & Calzetti, D. 1995, *AJ*, 110, 1071, doi: [10.1086/117587](https://doi.org/10.1086/117587)
- Conroy, C. 2013, *Annual Review of Astronomy and Astrophysics*, 51, 393455, doi: [10.1146/annurev-astro-082812-141017](https://doi.org/10.1146/annurev-astro-082812-141017)
- Crain, R. A., Schaye, J., Bower, R. G., et al. 2015, *MNRAS*, 450, 1937, doi: [10.1093/mnras/stv725](https://doi.org/10.1093/mnras/stv725)
- de Jong, R. S., Agertz, O., Berbel, A. A., et al. 2019, *The Messenger*, 175, 3, doi: [10.18727/0722-6691/5117](https://doi.org/10.18727/0722-6691/5117)
- Genel, S., Vogelsberger, M., Springel, V., et al. 2014, *MNRAS*, 445, 175, doi: [10.1093/mnras/stu1654](https://doi.org/10.1093/mnras/stu1654)
- Gladders, M. D., Oemler, A., Dressler, A., et al. 2013, *The Astrophysical Journal*, 770, 64, doi: [10.1088/0004-637X/770/1/64](https://doi.org/10.1088/0004-637X/770/1/64)
- Gratier, P., Bron, E., Gerin, M., et al. 2017, *A&A*, 599, A100, doi: [10.1051/0004-6361/201629847](https://doi.org/10.1051/0004-6361/201629847)
- Hamaus, N., Seljak, U., Desjacques, V., Smith, R. E., & Baldauf, T. 2010, *Physical Review D*, 82, doi: [10.1103/physrevd.82.043515](https://doi.org/10.1103/physrevd.82.043515)
- Harris, C. R., Millman, K. J., van der Walt, S. J., et al. 2020, *Nature*, 585, 357362, doi: [10.1038/s41586-020-2649-2](https://doi.org/10.1038/s41586-020-2649-2)
- Heavens, A., Panter, B., Jimenez, R., & Dunlop, J. 2004, *Nature*, 428, 625, doi: [10.1038/nature02474](https://doi.org/10.1038/nature02474)
- Hunter, J. D. 2007, *Computing in Science and Engineering*, 9, 90, doi: [10.1109/MCSE.2007.55](https://doi.org/10.1109/MCSE.2007.55)
- Jain, S., Tacchella, S., & Mosleh, M. 2024, *MNRAS*, 527, 3291, doi: [10.1093/mnras/stad3333](https://doi.org/10.1093/mnras/stad3333)
- Jones, P. A., Burton, M. G., Cunningham, M. R., et al. 2012, *MNRAS*, 419, 2961, doi: [10.1111/j.1365-2966.2011.19941.x](https://doi.org/10.1111/j.1365-2966.2011.19941.x)
- Joshi, G. D., Pillepich, A., Nelson, D., et al. 2021, *MNRAS*, 508, 1652, doi: [10.1093/mnras/stab2573](https://doi.org/10.1093/mnras/stab2573)
- Kauffmann, G. 2014, *Monthly Notices of the Royal Astronomical Society*, 441, 2717, doi: [10.1093/mnras/stu752](https://doi.org/10.1093/mnras/stu752)
- Kaushal, Y., Nersesian, A., Bezanson, R., et al. 2023, *arXiv e-prints*, arXiv:2307.03725, doi: [10.48550/arXiv.2307.03725](https://doi.org/10.48550/arXiv.2307.03725)
- Le Borgne, J. F., Bruzual, G., Pelló, R., et al. 2003, *A&A*, 402, 433, doi: [10.1051/0004-6361:20030243](https://doi.org/10.1051/0004-6361:20030243)
- Lee, B., Giallisco, M., Whitaker, K., et al. 2018, *ApJ*, 853, 131, doi: [10.3847/1538-4357/aaa40f](https://doi.org/10.3847/1538-4357/aaa40f)
- Leja, J., Carnall, A. C., Johnson, B. D., Conroy, C., & Speagle, J. S. 2019, *ApJ*, 876, 3, doi: [10.3847/1538-4357/ab133c](https://doi.org/10.3847/1538-4357/ab133c)
- Lo, N., Cunningham, M. R., Jones, P. A., et al. 2009, *MNRAS*, 395, 1021, doi: [10.1111/j.1365-2966.2009.14594.x](https://doi.org/10.1111/j.1365-2966.2009.14594.x)
- Lu, Z., Mo, H. J., Lu, Y., et al. 2014, *Monthly Notices of the Royal Astronomical Society*, 439, 1294, doi: [10.1093/mnras/stu016](https://doi.org/10.1093/mnras/stu016)
- . 2015, *Monthly Notices of the Royal Astronomical Society*, 450, 1604, doi: [10.1093/mnras/stv667](https://doi.org/10.1093/mnras/stv667)
- Madau, P., & Dickinson, M. 2014, *Annual Review of Astronomy and Astrophysics*, 52, 415486, doi: [10.1146/annurev-astro-081811-125615](https://doi.org/10.1146/annurev-astro-081811-125615)
- Marinacci, F., Vogelsberger, M., Pakmor, R., et al. 2018, *Monthly Notices of the Royal Astronomical Society*, doi: [10.1093/mnras/sty2206](https://doi.org/10.1093/mnras/sty2206)
- Melnick, G. J., Tolls, V., Snell, R. L., et al. 2011, *ApJ*, 727, 13, doi: [10.1088/0004-637X/727/1/13](https://doi.org/10.1088/0004-637X/727/1/13)
- Naiman, J. P., Pillepich, A., Springel, V., et al. 2018, *Monthly Notices of the Royal Astronomical Society*, 477, 1206, doi: [10.1093/mnras/sty618](https://doi.org/10.1093/mnras/sty618)
- Narayanan, D., Lower, S., Torrey, P., et al. 2023. <https://arxiv.org/abs/2306.10118>
- Nelson, D., Pillepich, A., Springel, V., et al. 2017, *Monthly Notices of the Royal Astronomical Society*, 475, 624, doi: [10.1093/mnras/stx3040](https://doi.org/10.1093/mnras/stx3040)
- Neufeld, D. A., Hollenbach, D. J., Kaufman, M. J., et al. 2007, *ApJ*, 664, 890, doi: [10.1086/518857](https://doi.org/10.1086/518857)
- Newville, M., Otten, R., Nelson, A., et al. 2023, *lmfit/lmfit-py: 1.2.2*, Tech. rep., doi: [10.5281/zenodo.8145703](https://doi.org/10.5281/zenodo.8145703)
- Pacifici, C., da Cunha, E., Charlot, S., et al. 2015, *MNRAS*, 447, 786, doi: [10.1093/mnras/stu2447](https://doi.org/10.1093/mnras/stu2447)
- Pacifici, C., Kassin, S. A., Weiner, B. J., et al. 2016, *ApJ*, 832, 79, doi: [10.3847/0004-637X/832/1/79](https://doi.org/10.3847/0004-637X/832/1/79)
- pandas development team, T. 2024, *pandas-dev/pandas: Pandas, v2.2.2*, Zenodo, doi: [10.5281/zenodo.10957263](https://doi.org/10.5281/zenodo.10957263)
- Pedregosa, F., Varoquaux, G., Gramfort, A., et al. 2011, *Journal of Machine Learning Research*, 12, 2825
- Peng, Y.-j., Lilly, S. J., Kovač, K., et al. 2010, *ApJ*, 721, 193, doi: [10.1088/0004-637X/721/1/193](https://doi.org/10.1088/0004-637X/721/1/193)
- Pillepich, A., Nelson, D., Hernquist, L., et al. 2017a, *Monthly Notices of the Royal Astronomical Society*, 475, 648, doi: [10.1093/mnras/stx3112](https://doi.org/10.1093/mnras/stx3112)
- Pillepich, A., Springel, V., Nelson, D., et al. 2017b, *Monthly Notices of the Royal Astronomical Society*, 473, 4077, doi: [10.1093/mnras/stx2656](https://doi.org/10.1093/mnras/stx2656)

- Planck Collaboration, Ade, P. A. R., Aghanim, N., et al. 2014, *Astronomy & Astrophysics*, 571, A1, doi: [10.1051/0004-6361/201321529](https://doi.org/10.1051/0004-6361/201321529)
- . 2016, *Astronomy & Astrophysics*, 594, A13, doi: [10.1051/0004-6361/201525830](https://doi.org/10.1051/0004-6361/201525830)
- Reddy, N. A., Pettini, M., Steidel, C. C., et al. 2012, *ApJ*, 754, 25, doi: [10.1088/0004-637X/754/1/25](https://doi.org/10.1088/0004-637X/754/1/25)
- Schaye, J., Crain, R. A., Bower, R. G., et al. 2014, *Monthly Notices of the Royal Astronomical Society*, 446, 521554, doi: [10.1093/mnras/stu2058](https://doi.org/10.1093/mnras/stu2058)
- Sijacki, D., Vogelsberger, M., Genel, S., et al. 2015, *MNRAS*, 452, 575, doi: [10.1093/mnras/stv1340](https://doi.org/10.1093/mnras/stv1340)
- Springel, V. 2005, *Monthly Notices of the Royal Astronomical Society*, 364, 11051134, doi: [10.1111/j.1365-2966.2005.09655.x](https://doi.org/10.1111/j.1365-2966.2005.09655.x)
- Springel, V. 2010, *MNRAS*, 401, 791, doi: [10.1111/j.1365-2966.2009.15715.x](https://doi.org/10.1111/j.1365-2966.2009.15715.x)
- Springel, V., Pakmor, R., Pillepich, A., et al. 2017, *Monthly Notices of the Royal Astronomical Society*, 475, 676, doi: [10.1093/mnras/stx3304](https://doi.org/10.1093/mnras/stx3304)
- Suess, K. A., Leja, J., Johnson, B. D., et al. 2022, *The Astrophysical Journal*, 935, 146, doi: [10.3847/1538-4357/ac82b0](https://doi.org/10.3847/1538-4357/ac82b0)
- Takada, M., Ellis, R. S., Chiba, M., et al. 2014, *PASJ*, 66, R1, doi: [10.1093/pasj/pst019](https://doi.org/10.1093/pasj/pst019)
- Tegmark, M., & Bromley, B. C. 1999, *ApJL*, 518, L69, doi: [10.1086/312068](https://doi.org/10.1086/312068)
- Thomas, D., Maraston, C., Bender, R., & Mendes de Oliveira, C. 2005, *ApJ*, 621, 673, doi: [10.1086/426932](https://doi.org/10.1086/426932)
- Ting, Y. S., Freeman, K. C., Kobayashi, C., De Silva, G. M., & Bland-Hawthorn, J. 2012, *Monthly Notices of the Royal Astronomical Society*, 421, 12311255, doi: [10.1111/j.1365-2966.2011.20387.x](https://doi.org/10.1111/j.1365-2966.2011.20387.x)
- Ungerechts, H., Bergin, E. A., Goldsmith, P. F., et al. 1997, *ApJ*, 482, 245, doi: [10.1086/304110](https://doi.org/10.1086/304110)
- Virtanen, P., Gommers, R., Oliphant, T. E., et al. 2020, *Nature Methods*, 17, 261272, doi: [10.1038/s41592-019-0686-2](https://doi.org/10.1038/s41592-019-0686-2)
- Vogelsberger, M., Genel, S., Springel, V., et al. 2014a, *Nature*, 509, 177, doi: [10.1038/nature13316](https://doi.org/10.1038/nature13316)
- . 2014b, *MNRAS*, 444, 1518, doi: [10.1093/mnras/stu1536](https://doi.org/10.1093/mnras/stu1536)
- Weinberger, R., Springel, V., Hernquist, L., et al. 2016, *Monthly Notices of the Royal Astronomical Society*, 465, 3291, doi: [10.1093/mnras/stw2944](https://doi.org/10.1093/mnras/stw2944)
- Weisz, D. R., Dalcanton, J. J., Williams, B. F., et al. 2011, *The Astrophysical Journal*, 739, 5, doi: [10.1088/0004-637x/739/1/5](https://doi.org/10.1088/0004-637x/739/1/5)
- Wild, V., Budavári, T., Blaizot, J., et al. 2008, in *American Institute of Physics Conference Series*, Vol. 1082, *Classification and Discovery in Large Astronomical Surveys*, ed. C. A. L. Bailer-Jones (AIP), 119–125, doi: [10.1063/1.3059021](https://doi.org/10.1063/1.3059021)
- Wong, A. W. C., & Taylor, J. E. 2012, *ApJ*, 757, 102, doi: [10.1088/0004-637X/757/1/102](https://doi.org/10.1088/0004-637X/757/1/102)
- Wu, P.-F., van der Wel, A., Gallazzi, A., et al. 2018, *ApJ*, 855, 85, doi: [10.3847/1538-4357/aab0a6](https://doi.org/10.3847/1538-4357/aab0a6)
- Yip, C. W., Connolly, A. J., Szalay, A. S., et al. 2004, *The Astronomical Journal*, 128, 585609, doi: [10.1086/422429](https://doi.org/10.1086/422429)
- Zhou, S., Li, C., Hao, C.-N., et al. 2021, *The Astrophysical Journal*, 916, 38, doi: [10.3847/1538-4357/ac06cc](https://doi.org/10.3847/1538-4357/ac06cc)
- Zhou, S., Merrifield, M., & Aragón-Salamanca, A. 2022, *MNRAS*, 513, 5446, doi: [10.1093/mnras/stac1279](https://doi.org/10.1093/mnras/stac1279)
- Zhou, S., Mo, H. J., Li, C., Boquien, M., & Rossi, G. 2020, *Monthly Notices of the Royal Astronomical Society*, 497, 4753, doi: [10.1093/mnras/staa2337](https://doi.org/10.1093/mnras/staa2337)
- Zhou, S., Zhang, P., & Chen, Z. 2023, *Monthly Notices of the Royal Astronomical Society*, 523, 57895798, doi: [10.1093/mnras/stad1824](https://doi.org/10.1093/mnras/stad1824)
- Zhou, S., Mo, H. J., Li, C., et al. 2019, *Monthly Notices of the Royal Astronomical Society*, 485, 5256, doi: [10.1093/mnras/stz764](https://doi.org/10.1093/mnras/stz764)
- Zibetti, S., Rossi, E., & Gallazzi, A. R. 2024, *Monthly Notices of the Royal Astronomical Society*, 528, 27902804, doi: [10.1093/mnras/stae178](https://doi.org/10.1093/mnras/stae178)

APPENDIX

A. PCA-BASED MODEL EIGEN-HISTORIES

In Table 2, we provide the empirical mean vector, as well as the first 10 eigen-histories of the PCA-based models. The first column is the look-back time from the present time to $z \lesssim 6$, and the second column is the empirical mean vector from TNG100. To implement the PCA+step model, one can replace the SFR during the past 300 million years from the PCA model with a step function.

Table 2. PCA-based SFH model base functions. The look-back time, shown in the first column, is sampled in a logarithmic scale (base 10). The following columns are the empirical mean vector, as well as the first 10 eigen-histories, both in linear scale. The PCA+step model uses the same empirical mean vector and eigen-histories here.

Lookback time [Gyr]	Mean	PC1	PC2	PC3	PC4	PC5	PC6	PC7	PC8	PC9	PC10
0.000	2.020	0.112	0.084	0.090	-0.083	-0.085	-0.068	0.070	-0.083	-0.079	-0.051
0.027	2.032	0.114	0.087	0.094	-0.085	-0.087	-0.069	0.071	-0.083	-0.079	-0.048
0.055	2.043	0.115	0.090	0.098	-0.087	-0.090	-0.071	0.073	-0.083	-0.079	-0.044
0.083	2.056	0.117	0.094	0.101	-0.089	-0.092	-0.073	0.074	-0.083	-0.079	-0.041
0.112	2.068	0.118	0.097	0.105	-0.091	-0.095	-0.075	0.076	-0.084	-0.079	-0.037
0.142	2.079	0.119	0.100	0.109	-0.093	-0.096	-0.075	0.076	-0.082	-0.077	-0.033
0.173	2.080	0.120	0.102	0.110	-0.091	-0.094	-0.070	0.070	-0.073	-0.070	-0.025
0.204	2.081	0.120	0.104	0.111	-0.090	-0.091	-0.064	0.065	-0.063	-0.061	-0.017
0.237	2.082	0.121	0.106	0.113	-0.088	-0.088	-0.059	0.059	-0.053	-0.053	-0.009
0.270	2.084	0.121	0.109	0.114	-0.086	-0.085	-0.053	0.052	-0.043	-0.045	-0.000
0.304	2.085	0.122	0.111	0.115	-0.085	-0.083	-0.047	0.046	-0.033	-0.036	0.009
0.339	2.086	0.122	0.113	0.117	-0.083	-0.080	-0.041	0.040	-0.022	-0.027	0.018
0.376	2.089	0.123	0.112	0.113	-0.073	-0.067	-0.027	0.022	0.001	-0.004	0.030
0.413	2.092	0.123	0.112	0.110	-0.064	-0.054	-0.012	0.004	0.024	0.019	0.042
0.451	2.095	0.123	0.111	0.106	-0.054	-0.040	0.004	-0.014	0.048	0.044	0.054
0.490	2.098	0.123	0.109	0.101	-0.043	-0.027	0.018	-0.031	0.068	0.063	0.064
0.530	2.101	0.123	0.107	0.094	-0.033	-0.014	0.031	-0.042	0.078	0.072	0.066
0.571	2.104	0.123	0.104	0.087	-0.022	-0.001	0.044	-0.055	0.089	0.081	0.069
0.613	2.107	0.123	0.101	0.080	-0.011	0.013	0.057	-0.067	0.101	0.090	0.072
0.657	2.110	0.122	0.098	0.072	0.001	0.027	0.071	-0.080	0.112	0.099	0.075
0.701	2.109	0.122	0.095	0.064	0.012	0.039	0.081	-0.088	0.117	0.101	0.073
0.747	2.105	0.121	0.091	0.056	0.022	0.052	0.088	-0.091	0.115	0.097	0.067
0.794	2.101	0.120	0.087	0.048	0.032	0.064	0.096	-0.095	0.112	0.093	0.060
0.842	2.105	0.119	0.083	0.039	0.043	0.075	0.102	-0.096	0.106	0.083	0.051
0.892	2.112	0.119	0.080	0.030	0.055	0.085	0.107	-0.096	0.098	0.071	0.039
0.943	2.120	0.119	0.076	0.021	0.068	0.095	0.113	-0.096	0.090	0.058	0.027
0.995	2.128	0.119	0.073	0.012	0.081	0.106	0.119	-0.096	0.081	0.045	0.015
1.049	2.130	0.119	0.068	0.003	0.090	0.113	0.119	-0.088	0.067	0.027	0.002
1.104	2.131	0.118	0.063	-0.007	0.099	0.118	0.117	-0.077	0.050	0.007	-0.013
1.161	2.136	0.117	0.058	-0.017	0.109	0.122	0.113	-0.064	0.031	-0.014	-0.026
1.219	2.149	0.117	0.055	-0.028	0.119	0.125	0.104	-0.047	0.007	-0.038	-0.038
1.279	2.163	0.117	0.051	-0.039	0.129	0.127	0.095	-0.030	-0.018	-0.063	-0.050
1.340	2.177	0.118	0.047	-0.050	0.140	0.130	0.085	-0.012	-0.044	-0.088	-0.062
1.403	2.190	0.117	0.042	-0.060	0.145	0.125	0.069	0.012	-0.064	-0.106	-0.064

1.468	2.204	0.117	0.037	-0.071	0.149	0.120	0.054	0.035	-0.085	-0.124	-0.066
1.534	2.204	0.116	0.030	-0.078	0.149	0.109	0.033	0.054	-0.097	-0.126	-0.057
1.603	2.203	0.115	0.024	-0.087	0.148	0.099	0.012	0.074	-0.109	-0.128	-0.047
1.673	2.204	0.114	0.017	-0.094	0.147	0.087	-0.009	0.092	-0.118	-0.126	-0.034
1.745	2.213	0.112	0.011	-0.100	0.139	0.068	-0.031	0.103	-0.112	-0.103	-0.012
1.819	2.222	0.111	0.004	-0.106	0.132	0.048	-0.053	0.114	-0.106	-0.078	0.012
1.894	2.227	0.109	-0.002	-0.112	0.125	0.029	-0.075	0.122	-0.095	-0.052	0.033
1.972	2.229	0.107	-0.009	-0.118	0.120	0.010	-0.096	0.127	-0.079	-0.023	0.052
2.052	2.250	0.107	-0.014	-0.124	0.114	-0.009	-0.113	0.128	-0.057	0.008	0.077
2.135	2.274	0.108	-0.019	-0.130	0.108	-0.029	-0.131	0.128	-0.033	0.041	0.104
2.219	2.291	0.107	-0.025	-0.135	0.100	-0.051	-0.144	0.118	-0.005	0.072	0.121
2.306	2.303	0.106	-0.030	-0.137	0.090	-0.075	-0.152	0.101	0.027	0.098	0.127
2.395	2.311	0.104	-0.036	-0.137	0.076	-0.092	-0.147	0.075	0.057	0.107	0.112
2.486	2.319	0.103	-0.041	-0.137	0.060	-0.109	-0.142	0.049	0.087	0.116	0.095
2.580	2.338	0.102	-0.046	-0.136	0.046	-0.125	-0.129	0.018	0.109	0.114	0.076
2.676	2.355	0.100	-0.051	-0.135	0.031	-0.140	-0.114	-0.015	0.130	0.111	0.055
2.775	2.341	0.097	-0.059	-0.134	0.017	-0.145	-0.094	-0.047	0.143	0.096	0.026
2.877	2.361	0.096	-0.066	-0.135	0.001	-0.155	-0.067	-0.076	0.145	0.070	-0.009
2.981	2.386	0.096	-0.074	-0.136	-0.015	-0.165	-0.040	-0.104	0.144	0.040	-0.044
3.089	2.390	0.093	-0.081	-0.131	-0.031	-0.167	-0.015	-0.122	0.133	-0.004	-0.072
3.199	2.410	0.092	-0.088	-0.126	-0.048	-0.166	0.015	-0.137	0.115	-0.049	-0.091
3.312	2.437	0.091	-0.093	-0.120	-0.065	-0.156	0.048	-0.142	0.084	-0.087	-0.092
3.428	2.437	0.088	-0.097	-0.110	-0.077	-0.139	0.081	-0.138	0.040	-0.116	-0.081
3.547	2.457	0.086	-0.102	-0.102	-0.091	-0.121	0.116	-0.133	-0.004	-0.143	-0.068
3.669	2.500	0.084	-0.109	-0.096	-0.104	-0.104	0.146	-0.123	-0.045	-0.152	-0.047
3.795	2.516	0.080	-0.115	-0.086	-0.115	-0.086	0.168	-0.107	-0.081	-0.143	-0.017
3.924	2.533	0.079	-0.117	-0.074	-0.124	-0.068	0.183	-0.080	-0.115	-0.125	0.031
4.057	2.545	0.075	-0.118	-0.063	-0.129	-0.046	0.188	-0.047	-0.135	-0.093	0.079
4.193	2.541	0.072	-0.121	-0.051	-0.133	-0.020	0.186	-0.002	-0.146	-0.043	0.123
4.333	2.565	0.069	-0.125	-0.039	-0.136	0.006	0.182	0.045	-0.148	0.014	0.157
4.476	2.597	0.067	-0.129	-0.027	-0.136	0.032	0.173	0.091	-0.136	0.070	0.170
4.624	2.627	0.064	-0.132	-0.013	-0.134	0.058	0.153	0.132	-0.105	0.116	0.159
4.775	2.678	0.061	-0.136	0.001	-0.134	0.082	0.121	0.166	-0.059	0.152	0.126
4.931	2.661	0.056	-0.134	0.016	-0.124	0.105	0.091	0.188	-0.005	0.164	0.072
5.091	2.743	0.055	-0.139	0.029	-0.127	0.129	0.063	0.216	0.052	0.169	0.010
5.255	2.766	0.050	-0.143	0.041	-0.125	0.143	0.030	0.223	0.107	0.140	-0.052
5.423	2.796	0.047	-0.144	0.054	-0.110	0.148	-0.012	0.189	0.156	0.072	-0.102
5.596	2.802	0.042	-0.141	0.066	-0.090	0.143	-0.050	0.142	0.183	-0.010	-0.124
5.773	2.835	0.039	-0.139	0.079	-0.072	0.144	-0.083	0.092	0.196	-0.086	-0.117
5.956	2.898	0.034	-0.138	0.095	-0.052	0.141	-0.115	0.036	0.202	-0.161	-0.091
6.143	2.958	0.028	-0.140	0.105	-0.027	0.136	-0.141	-0.021	0.196	-0.224	-0.037
6.335	3.023	0.024	-0.138	0.110	-0.008	0.121	-0.148	-0.068	0.144	-0.228	0.039
6.533	3.036	0.016	-0.137	0.115	0.006	0.097	-0.141	-0.106	0.081	-0.188	0.115
6.736	3.082	0.009	-0.135	0.122	0.022	0.084	-0.138	-0.134	0.024	-0.152	0.182
6.944	3.143	-0.000	-0.132	0.136	0.047	0.064	-0.134	-0.161	-0.038	-0.113	0.241
7.158	3.170	-0.006	-0.121	0.137	0.067	0.037	-0.116	-0.163	-0.093	-0.046	0.242
7.378	3.204	-0.015	-0.115	0.142	0.092	0.008	-0.098	-0.167	-0.149	0.031	0.228
7.603	3.216	-0.022	-0.104	0.138	0.108	-0.026	-0.071	-0.143	-0.162	0.090	0.142
7.835	3.225	-0.033	-0.090	0.140	0.127	-0.059	-0.036	-0.115	-0.165	0.144	0.058
8.073	3.237	-0.040	-0.076	0.140	0.146	-0.091	-0.002	-0.083	-0.154	0.176	-0.040

8.317	3.242	-0.045	-0.067	0.130	0.145	-0.091	0.023	-0.045	-0.103	0.149	-0.100
8.568	3.252	-0.056	-0.054	0.120	0.143	-0.105	0.057	0.000	-0.056	0.113	-0.138
8.826	3.300	-0.072	-0.036	0.116	0.155	-0.135	0.100	0.051	-0.011	0.074	-0.181
9.090	3.293	-0.083	-0.017	0.101	0.149	-0.144	0.118	0.095	0.045	0.017	-0.141
9.362	3.272	-0.095	0.001	0.085	0.142	-0.150	0.138	0.130	0.094	-0.045	-0.109
9.641	3.259	-0.104	0.022	0.065	0.132	-0.150	0.146	0.140	0.111	-0.077	-0.007
9.927	3.227	-0.110	0.041	0.045	0.114	-0.139	0.146	0.139	0.124	-0.098	0.093
10.222	3.176	-0.123	0.074	0.014	0.085	-0.125	0.143	0.141	0.141	-0.149	0.222
10.524	3.097	-0.130	0.106	-0.020	0.040	-0.085	0.116	0.129	0.143	-0.172	0.265
10.834	3.007	-0.141	0.130	-0.054	0.004	-0.051	0.086	0.101	0.121	-0.145	0.254
11.153	2.894	-0.152	0.174	-0.110	-0.054	0.004	0.038	0.050	0.097	-0.122	0.228
11.480	2.716	-0.157	0.221	-0.173	-0.136	0.079	-0.035	-0.028	0.023	-0.042	0.130
11.816	2.398	-0.141	0.223	-0.193	-0.176	0.130	-0.091	-0.091	-0.048	0.040	0.004
12.161	1.935	-0.116	0.198	-0.184	-0.188	0.158	-0.129	-0.135	-0.103	0.108	-0.103
12.515	1.255	-0.069	0.123	-0.120	-0.129	0.113	-0.095	-0.099	-0.084	0.087	-0.104
12.879	0.502	-0.028	0.048	-0.046	-0.050	0.044	-0.039	-0.041	-0.037	0.038	-0.048

B. TEST RESULTS FOR USING DIFFERENT NUMBERS OF EIGEN-HISTORIES

In §3, we present the PVE test of the PCA-based models. There we find that the cumulative data variance explained by the first few eigen-histories increases the fastest, and that the first 5 eigen-histories can capture $\sim 65\%$ of the data variances. Here, we study the effects of using a different number of eigen-histories quantitatively in both the SFH and spectral spaces. The results obtained from the entire sample of 9168 TNG100 central galaxies are shown in Fig. 11. In both panels, we show the median Δ values using solid lines and the 25 - 75 percentile values using dashed lines.

In the SFH space (left panel), it is seen that as the number of eigen-histories used in each model increases, the median Δ_{SFH} value gradually decreases. This is expected since when more higher-order eigen-histories are used, more small-scale details can be recovered, thus making the best-fit SFHs closer to the input SFHs. Similarly to the PVE test, within the first few eigen-histories, the median Δ_{SFH} curves are steeper. The similar performance of the two PCA-based models is also expected.

On the contrary, the statistical performance becomes more diverse in the spectral space, as shown in the right-hand side panel of Fig. 11. Again, as the number of eigen-histories increases, the spectra generated by the best-fit SFHs better match the input mock spectra generated by the input SFHs. However, when comparing the models with the same number of eigen-histories, the median Δ_{spec} values of the PCA+step model are roughly an order of magnitude smaller. Clearly, the effects on the spectral shape come from the most recent star formation (within the past $\sim 0.3\text{Gyr}$). Furthermore, the decreasing trends become much shallower after the first 5 eigen-histories. This is because the higher-order components govern the high-frequency details of the SFHs, which are not well reflected in the spectra. In particular, from the PCA+step model, the median Δ_{spec} becomes quite flat starting from the 5th eigen-history. Thus, we argue that using the first 5 eigen-histories in our PCA-based models is sufficient to model the overall properties of galaxy spectra.

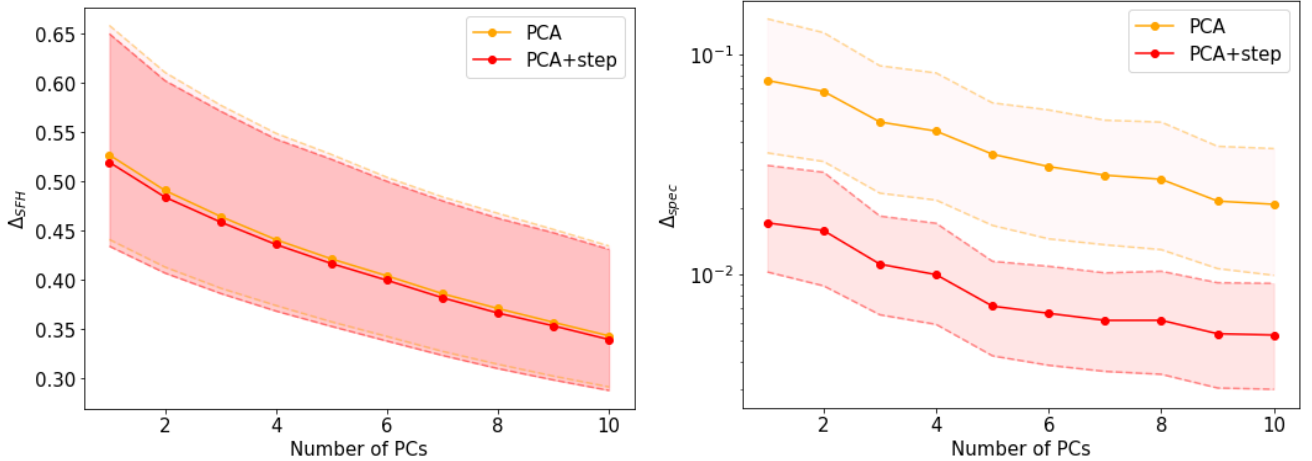


Figure 11. The Δ values of the PCA model (orange) and the PCA+step model (red) obtained by using the first 1 to 10 eigen-histories. The solid curves mark the median Δ values, while the dashed curves mark the 25 and 75 percentile values. The left and right panels show Δ_{SFH} and Δ_{spec} , respectively.